Impact of the 50 Hz harmonics on the beam evolution of the Large Hadron Collider

S. Kostoglou*
CERN, Geneva 1211, Switzerland
and
National Technical University of Athens, Athens 15780, Greece

G. Arduini, Y. Papaphilippou, and G. Sterbini
CERN, Geneva 1211, Switzerland

L. Intelisano
CERN, Geneva 1211, Switzerland
and
INFN, Sapienza Università di Roma, Rome 00185, Italy

(Dated: December 10, 2021)

Since the beginning of the Large Hadron Collider (LHC) commissioning, spectral components at harmonics of the mains frequency (50 Hz) have been observed in the transverse beam spectrum. This paper presents an overview of the most important observations, collected during the latest physics operation of the LHC in 2018, which clearly indicates that the harmonics are the result of a real beam excitation rather than an instrumental feature. Based on these findings, potential sources of the perturbation are discussed and a correlation with noise originating from the magnets' power converters is presented. As many of these tones reside in the vicinity of the betatron tune, they can increase the diffusion of the particles in the distribution in the presence of non-linear effects, leading to proton losses and eventually to a lifetime reduction. A quantitative characterization of the machine noise spectrum, together with an understanding of the noise source is an essential ingredient to evaluate the impact of the 50 Hz harmonics on the future upgrade of the LHC, the High Luminosity LHC (HL-LHC). To this end, simulations with the single-particle tracking code, SixTrack, are employed, including a realistic noise spectrum as extracted from experimental observations. The methods and results of the tracking studies are reported and discussed in this paper.

arXiv:2003.00140v3 [physics.acc-ph] 29 Mar 2020

I. INTRODUCTION

In particle accelerators, studies of the beam spectrum can reveal important information concerning the existence of external noise sources that perturb the motion of the particles. Noise effects, such as power supply ripples, ground motion and the noise induced by the transverse feedback system, are an important issue for the single-particle beam dynamics in past, present and future accelerators. In the presence of non-linearities, depending on the spectral components and the nature of the source, noise can act as a diffusion mechanism for the particles in the beam distribution, through the excitation of resonances in addition to the ones driven by the lattice non-linearities, an effect that can prove detrimental to the beam lifetime [1–4]. This paper focuses on the investigation of such a noise mechanism that has been observed in the beam spectrum of the Large Hadron Collider (LHC) [5], which is contaminated by harmonics of 50 Hz [6–9]. The aim of this study is to extend the understanding of the noise mechanisms that have been observed in the LHC and to determine whether the aforementioned mechanism can pose a limitation to the luminosity production in future operation.

Observations of harmonics of the mains power frequency in the beam spectrum have been reported in the past from several accelerators such as the Super Proton Synchrotron (SPS) at CERN [10–14], the Hadron-Electron Ring Accelerator (HERA) in Deutsches Elektronen-Synchrotron (DESY) [3, 15, 16], the Relativistic Heavy Ion Collider (RHIC) at Brookhaven National Laboratory (BNL) [17, 18] and the Tevatron in Fermi National Accelerator Laboratory (FNAL) [19, 20]. The past studies can be roughly divided into two categories: observations of harmonics in the transverse beam spectrum, first, in the form of dipolar perturbations, i.e., the frequency of the lines does not depend on the tune and, second, as a tune modulation, with the harmonics appearing as sidebands around the betatron tune. As far as the dipolar excitations are concerned, the studies in the SPS excluded the factor of instrumentation noise as the origin of the perturbation [10]. By computing the phase evolution of the noise lines between two consecutive bunches, it was shown that the beam was excited by high order harmonics, mainly affecting the horizontal plane. It was proven that one source of the perturbation was the main dipoles by injecting an external sinusoidal ripple on their power supply. The study con-

* sofia.kostoglou@cern.ch

ducted at RHIC demonstrated that high order harmonics ($h > 100$) were visible in several unrelated instruments as a result of a real beam excitation rather than an artifact of the instrumentation system [17]. To explore the origin of the perturbation, machine parameters such as the betatron tune and the coupling were modified and the source was identified as a dipolar field error. Through a set of experiments, a correlation with power converter noise was established and specifically, with the 12-pulse line-commutated thyristor power converters of the main dipoles [18]. During these tests, the phases of these power converters were modified, which led to distinct changes in the amplitude evolution of the lines. The SPS studies also revealed the existence of harmonics as sidebands around the betatron tune, resulting from power supply ripples in quadrupole magnets [11–13]. It was proven that the presence of multiple voltage tones arising from this effect led to increased losses and emittance growth compared to the single tone case due to the resonance overlap. In HERA, a novel tune ripple feedback system was applied as a compensation scheme for the quadrupolar power supply ripples [15, 16]. The working principle of the method was to inject a modulation with an equal amplitude and an opposite phase to the observed power supply ripples, which proved beneficial for the beam lifetime.

A similar observation of 50 Hz high order harmonics perturbing the beam spectrum in the form of a dipolar excitation is also systematically made in the LHC. In this paper, we present the analysis of the experimental data acquired during the 2018 LHC operation and the results of the tracking simulations aiming to identify the origin of the perturbation and to determine whether the observed noise leads to a degradation of the beam performance. Similarly to the aforementioned studies, the difficulty of the subject resides, first, in proving that the noise lines originate from the beam and not due to an artifact of the instrumentation systems and, second, in establishing a correlation with the origin of the perturbation. In the framework of this investigation, a thorough analysis of observations and dedicated experiments were conducted during the 2018 proton run. Based on the findings, the key observations that lead to the understanding that the harmonics are the result of a real beam excitation are presented in Section II. A potential correlation with noise arising from the power converters of the Main Bends is, first, investigated through parasitic observations and, then, for the first time in the LHC operation, it is confirmed with dedicated experiments. Furthermore, the impact of controlled dipolar excitations on the beam lifetime, conducted with the transverse damper, is described in Section III, which provides a tool for the validation of the Dynamic Aperture (DA) simulations in the presence of noise. The impact of the harmonics on the beam performance in terms of tune diffusion, DA and lifetime is discussed in the last section (Sec. IV), using a lumped noise model and a realistic noise spectrum. The LHC spectrum is then used to make projections for its future upgrade, the High Luminosity-LHC (HL-LHC) [21].

II. EXPERIMENTAL OBSERVATIONS

Throughout this paper, the main observable is the representation of the beam signal in frequency domain as computed with the Fast Fourier Transform (FFT). Based on the Fourier analysis, information concerning the origin of the 50 Hz can be extracted. This can be achieved by following the evolution of the lines in frequency domain, both in terms of amplitude and phase, during normal operation, i.e., without any modification in the beam or machine parameters (Sections II B). In this context, general observations acquired from various instruments are presented, providing a first insight on the subject under study. The need for high bandwidth measurements is explained, the distinct signature of the harmonics in frequency domain is illustrated and definitive proof of the noise coupling to the betatron motion is presented. Then, the findings are further extended by observing the response of the harmonics during modifications in the beam or machine configuration (Sections II C). These modifications refer to changes, first, in the betatron motion with parameters such as the tune, the phase advance and the beam energy, second, in the power converters and last, in the settings of the transverse damper.

A. Overview of the LHC beam modes

The fact that different beam energies and phases of the LHC nominal cycle have been explored in this study justifies the need to include a brief description of the beam modes that are relevant to the next sections of this paper. Figure 1 illustrates the operational cycle for a physics fill (Fill 7333). The different beam modes (gray) are presented along with the intensity evolution of Beam 1 (blue) and 2 (red) in the right axis and the beam energy (black) in the left axis. In brief, the nominal LHC cycle is organized as follows. After injecting low-intensity single bunches for machine protection reasons, high-intensity batches (two or three trains of 48 or 72 bunches and a bunch spacing of 25 ns) are injected from the SPS to the LHC rings until the requested filling scheme is reached. The *Injection* is performed in the Interaction Point (IP) 2 and 8 for Beam 1 and 2, respectively, with a total energy equal to 900 GeV. Then, during *Ramp*, the current of the main dipoles and quadrupoles increases while the beams are accelerated. An intermediate squeeze of the β-functions at the IPs, β^*, is performed [22]. At *Flat Top*, the beams have reached the maximum total energy of 13 TeV (as compared to the nominal design total energy of 14 TeV). After a few minutes, the betatron tunes are trimmed from the injection $(Q_x, Q_y) = (62.28, 60.31)$ to the collision $(Q_x, Q_y) = (62.31, 60.32)$ values (magenta). With the Achromatic Telescopic Squeezing (ATS) optics [23], the beams are squeezed to $\beta^* = 30$ cm at the IPs of

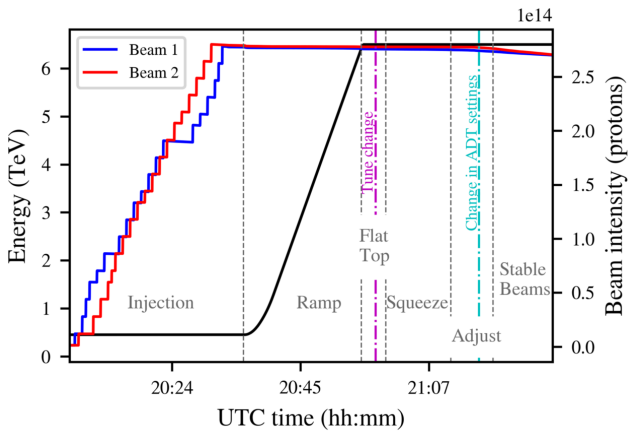

FIG. 1. The LHC operational cycle in 2018 (Fill 7333).

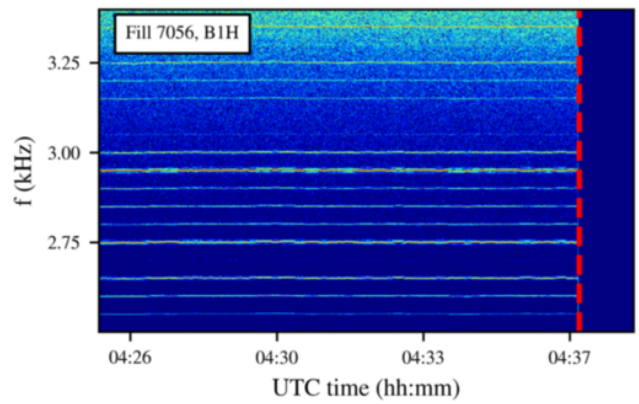

FIG. 2. Horizontal HS BBQ spectrogram of Beam 1 at the end of a physics fill (Fill 7056), centered around the 3 kHz frequency. The red dashed line indicates the end of the fill and the start of the dump of the beam.

the two high luminosity experiments (ATLAS and CMS). During *Adjust*, the separation bumps in the Interaction Regions (IRs) collapse and the beams are brought to collision. At the end of this beam mode, the settings of the transverse damper are modified (cyan). The declaration of *Stable Beams* signals the start of the data acquisition from the experiments. In this beam mode, luminosity optimization techniques are employed such as the crossing angle anti-leveling and the β^*-leveling [24, 25]. Finally, the beams are extracted from the ring to the dump.

B. Measurements in normal operation

This section presents the observations collected during constant beam and machine conditions and it is organized as follows. First, the spectrum at the end of a physics fill is presented, along with the beam spectrum acquired from multiple unrelated instruments. Then, the study focuses on the spectrum at Stable Beams, the frequency modulation of the harmonics and finally, their phase advance.

The first step is to illustrate the concept of the 50 Hz lines on the beam spectrum. To this end, the turn-by-turn data from the High Sensitivity Base-Band measurement system (HS BBQ) [26, 27] are extracted. For instance, Fig. 2 depicts the spectrogram of the horizontal plane of Beam 1 (Fill 7056) for the last few minutes of the fill, extending up to the first few minutes of the beam dump (red dashed line). The Fourier analysis for each time interval in the horizontal axis is performed with a window length of 2^{13} consecutive turns and an overlap of 2^{11} turns between windows. The frequency range is zoomed below the Beam 1 horizontal tune (≈3.49 kHz) to observe the 50 Hz harmonics in its proximity. A color code is assigned to the Power Spectral Density (PSD) to distinguish the main spectral components (yellow and red) from the noise baseline (blue).

The spectrum clearly shows that a series of 50 Hz harmonics are present in the beam signal. The fact that the lines appear as multiples of 50 Hz and not as sidebands around the betatron tune is one of the first indications among others (see Section II C) that the nature of the noise is dipolar. Furthermore, the harmonics are visible only in the presence of the beam. All signals acquired after the end of the fill are dominated by the noise of the instrument. A comparison between the signals prior and after the dump of the beam provides a first indication that the lines do not emerge as a result of instrumentation noise.

In an attempt to further exclude the factor of instrumental or environmental noise, the presence of these harmonics has been validated from different beam instruments. In this context, position measurements from multiple pickups, located in different positions in the LHC ring, are collected. The main observables are the HS BBQ, the transverse damper Observation Box (ADTObsBox) [28–30], the Diode Orbit and Oscillation System (DOROS) [31, 32] and the Multi-Band Instability Monitor (MIM) [33, 34]. Measurements from all the aforementioned instruments are available for the Machine Development (MD) Fill 7343, dedicated to studies concerning the 50 Hz harmonics. Figure 3 shows the spectra for the HS BBQ (Fig. 3a), the ADTObsBox (Fig. 3b), the MIM (Fig. 3c) and the DOROS (Fig. 3d) for the horizontal plane of Beam 1, while the vertical gray lines represent the multiples of 50 Hz. To illustrate that the lines in the beam spectrum correspond to 50 Hz harmonics, a zoomed region of the spectrum is depicted in Fig. 3a (light blue). As a reference, the sampling frequency and the number of turns (f_s, N) considered for each spectrum is $(f_{\text{rev}},\ 9000)$, $(3 \cdot f_{\text{rev}},\ 65536)$, $(16 \cdot f_{\text{rev}},\ 65536)$, $(f_{\text{rev}},\ 16384)$, respectively, where $f_{\text{rev}} = 11.245$ kHz is the LHC revolution frequency.

From the review of the spectra, it is confirmed that a series of 50 Hz harmonics is visible across several unrelated instruments. It should be mentioned that the

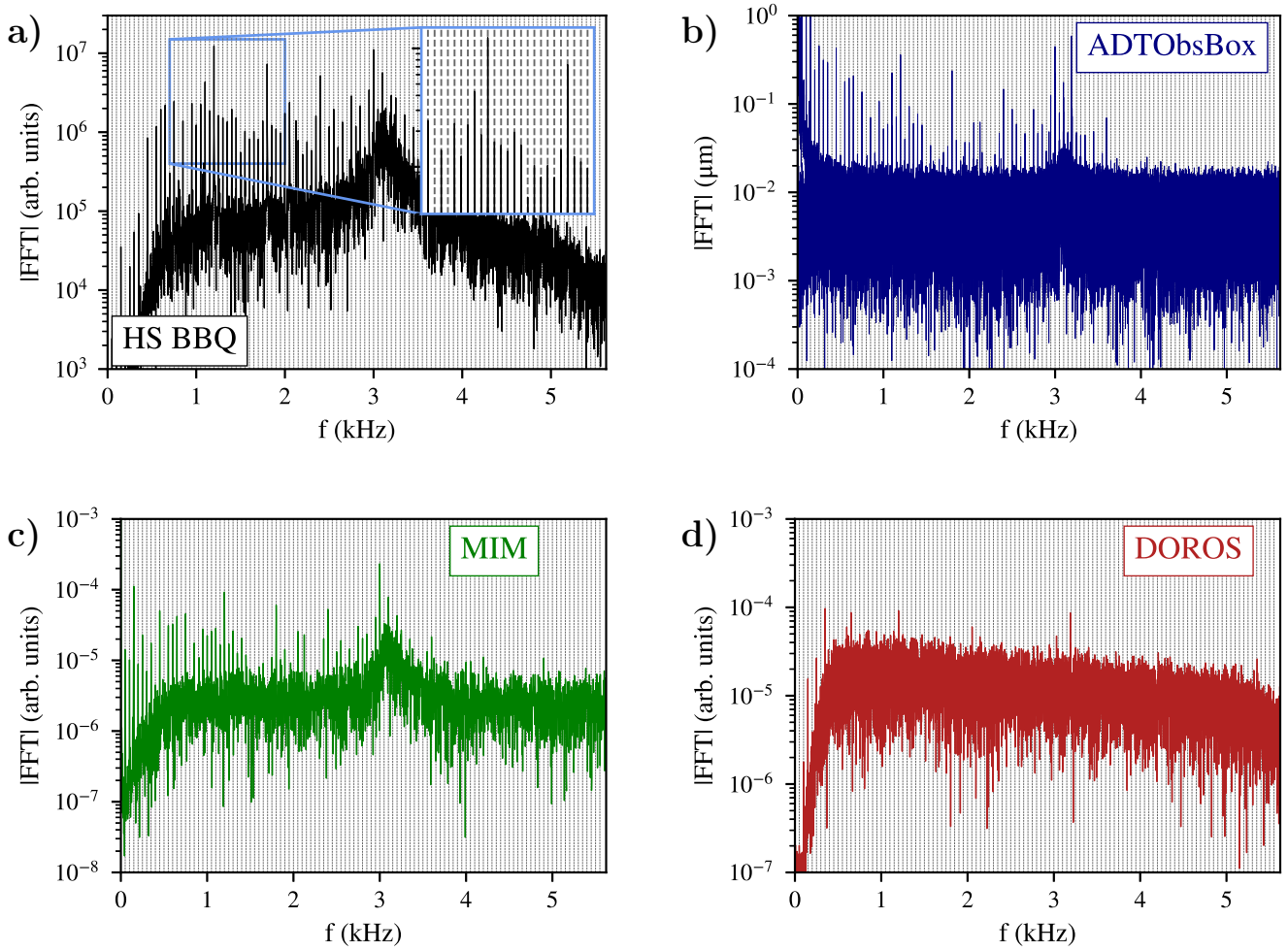

FIG. 3. The horizontal spectrum of Beam 1 at injection energy during the MD Fill 7343 from the (a) HS BBQ and with a zoomed window (light blue), (b) from the ADTObsBox, (c) MIM and (d) DOROS. The vertical gray lines represent the multiples of 50 Hz.

sampling rate, the window length, the noise floor and the frequency response of each pickup is different, which explains the observed discrepancies between the spectra in terms of resolution. For a consistent comparison of the acquisitions, the frequency range is limited to approximately 5.6 kHz, which is the Nyquist frequency of the turn-by-turn acquisitions, assuming a single observation point along the accelerator (the sampling frequency is $f_s = f_{\mathrm{rev}}$) [35].

For this study, it is of interest to investigate the range of 50 Hz harmonics visible in the beam signal. As mentioned above, the turn-by-turn acquisitions, such as the ones from the HS BBQ and DOROS, allow accessing a frequency regime up to 5.6 kHz. If present in the signal, frequency components beyond this limit will be aliased in the spectrum.

On the contrary, the ADTObsBox and the MIM provide high sampling rate measurements. Specifically, the ADTObsBox instability buffer contains calibrated bunch-by-bunch position measurements for 2^{16} turns. Firstly, the fact that a calibrated metric is provided allows computing the offsets induced on the beam motion from the 50 Hz harmonics. Secondly, the bunch-by-bunch information is needed to study the evolution of the 50 Hz in the cycle and to compute a high bandwidth spectrum, in the presence of a regular filling scheme. As shown in Appendix A, the noise floor of the single bunch ADTObsBox spectrum exceeds the amplitude of the 50 Hz harmonics and therefore, a decrease of the noise baseline is necessary to study their evolution during the cycle. To overcome this problem, a method to combine the information from several bunches has been developed, taking into account the dephasing of the spectrum, due to the time delay, across the different bunches (Appendix A). Assuming a regular filling scheme (equal spacing between bunches), this signal averaging algorithm not only provides a reduction of the noise floor but also extends the measurable frequency range of the beam spectrum, while

suppressing the aliases and preserving the signal metric. For all the reasons stated above, the ADTObsBox is the main observable in the following investigation. As far as these studies are concerned, the main limitation of this instrument is that regular acquisitions were not available in the last LHC physics run. In particular cases, where both consecutive acquisitions and a high bandwidth are required, the MIM measurements are used, at the expense of non-calibrated offsets.

The horizontal beam spectrum of Beam 2 is computed for the physics Fill 7334 during collisions, using the bunch-by-bunch and turn-by-turn acquisitions from the Q7 pickup of the ADTObsBox. Although only the spectrum of Beam 2 is depicted, similar observations exist for both beams and planes. Figure 4 illustrates the Fourier analysis, first, for a frequency range up to 10 kHz (Fig. 4a). From the review of the spectrum, two areas of particular interest are identified. The first regime (blue span) consists of 50 Hz harmonics extending up to 3.6 kHz. The second area (orange span) is a cluster of 50 Hz at 7-8 kHz. In particular, the cluster is centered at the frequency $f_{\mathrm{rev}} - f_x$, where f_x is the horizontal betatron frequency, which is ≈3.15 kHz at injection and ≈3.49 kHz at collision (see also Section II C). In the frequency interval between the two clusters, either no harmonics are present in the signal or their amplitude is below the noise threshold of the instrument. Throughout this paper, the two regimes of interest are referred to as the low and high-frequency cluster, respectively. It must be noted that the lowest order harmonics are excluded from the analysis as their amplitude is affected by the noise of the instrument. Then, the calibrated spectrum indicates that the harmonics of the high-frequency cluster are more important in terms of amplitude.

As the high-frequency cluster is situated at $f_{\mathrm{rev}} - f_x$, the question that naturally arises is whether these frequency components emerge from aliasing. In fact, even in the case of a physics fill, the sampling rate is only approximately uniform as not all trains are equally spaced. This error can give rise to the aliasing of the low-frequency cluster around the revolution frequency. It must be noted however, that the beam revolution frequency is not a multiple of 50 Hz and therefore, the aliases can be distinguished from the excitations at 50 Hz. Figure 4b presents the spectrum centered around the high-frequency cluster. The red dashed lines represent the expected position of aliased 50 Hz harmonics ($f_{\mathrm{rev}} - f_{50}$, where f_{50} are the harmonics of the low-frequency cluster, while the gray dashed lines illustrate the multiples of 50 Hz ($n \cdot f_{50}$, where n is a positive integer). As the spectral components of the high-frequency cluster coincide with the 50 Hz multiples, it is concluded that they are not aliased frequencies.

The time variation of the beam spectrum can reveal important information concerning the source of the perturbation. Due to the variation of the power grid load, the frequency of the mains power supply is not strictly 50 Hz. The study focuses on the impact of the aforementioned drift on the frequency evolution of the 50 Hz harmonics in order to illustrate their distinct signature in the frequency domain. Consecutive measurements are required for a detailed representation of the spectrograms and thus, as previously stated, the following analysis is based on the MIM and the HS BBQ acquisitions.

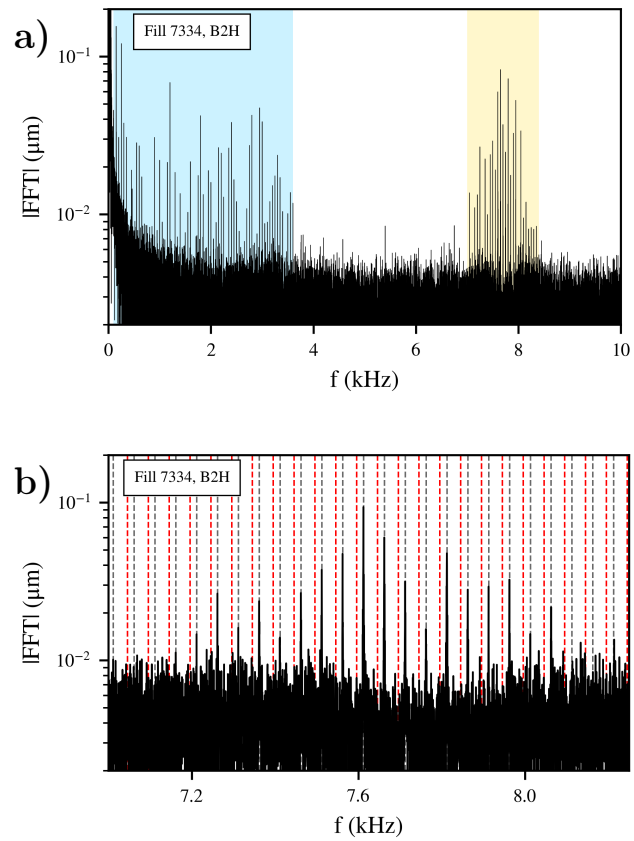

FIG. 4. The horizontal spectrum of Beam 2 at top energy for a frequency range up to 10 kHz (a), with the low and high-frequency cluster indicated by the blue and orange span, respectively, and centered around the high-frequency cluster (b). The red and gray dashed lines represent the expected position of aliased and physical 50 Hz harmonics, respectively.

The spectrogram of the horizontal position of Beam 1 is computed from the MIM data for a time interval at Stable Beams in the physics Fill 7256. In Fig. 5, the horizontal axis represents the timestamp of each spectrum with a window length of 2^{14} turns, the vertical axis is centered around a value in the low (left) and high (right) frequency cluster and a color code is assigned to the PSD. An important finding is that, although the lines are harmonics of 50 Hz, a time variation of their frequency is observed. Specifically, all harmonics are affected by a similar frequency modulation, the amplitude of which is proportional to the order of the harmonic. For this reason, the aforementioned effect is more pronounced in the harmonics of the high-frequency cluster, an observation which provides yet another indication that these compo-

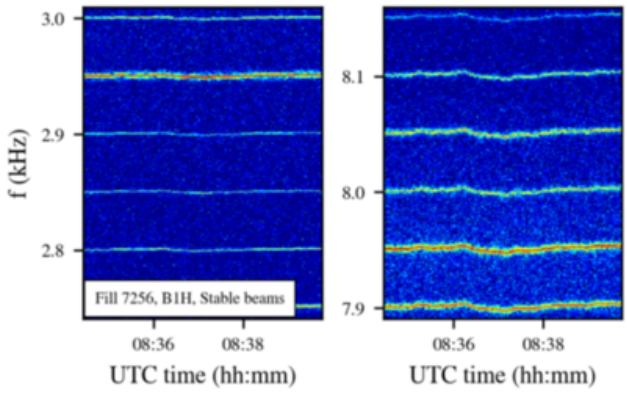

FIG. 5. The horizontal spectrogram of Beam 1 in a regime of the low (left) and high (right) frequency cluster.

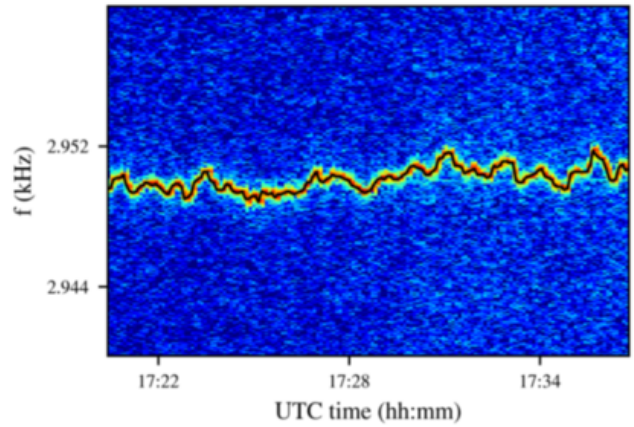

FIG. 6. The horizontal spectrogram of Beam 1 centered around 2.95 kHz and the frequency evolution of the harmonic (black curve) as computed from the maximization algorithm.

nents are not aliases.

To illustrate quantitatively that the harmonics experience a similar frequency modulation, the amplitude of which scales with the order of the harmonic, an algorithm that can precisely follow their evolution has been implemented. The steps of the algorithm are the following: for each measured time interval the amplitude of the Fourier spectrum is computed. The algorithm focuses on a regime in the vicinity of a single harmonic and, by employing a maximization routine, an accurate determination of its frequency is achieved by detecting the local maximum. The algorithm returns the frequency and the amplitude of the harmonic at each time step. This procedure is repeated for all the time intervals in the spectrogram. An example of the routine's result is depicted in Fig. 6. The spectrogram is centered around the 2.95 kHz line and the black line represents the frequency determination from the aforementioned method. The agreement between the results of the algorithm and the spectrogram proves that the frequency evolution of the harmonic is very well determined.

Iterating over all the harmonics in the spectrum with the aforementioned algorithm validates the existence of a similar frequency modulation with an amplitude proportional to the order of the harmonic. Figure 7 shows the frequency evolution of all the harmonics (black) after individually subtracting the mean value, normalizing with the order of the harmonic and projecting to the fundamental frequency (50 Hz). The modulation of the fundamental frequency and its low order harmonics cannot be directly extracted from the beam spectrum without a more refined analysis due to the limited resolution and hence, these components have been excluded. The modulation is visible in both beams and planes, during all beams modes and across several unrelated instruments. The proportional relationship between the modulation amplitude and the harmonic order, observed both in the low and high-frequency cluster, suggests that they emerge from a common source (see Appendix B).

The origin of the modulation is clearly related to the stability of the 50 Hz mains from the electrical network, which then propagates to all the harmonics. This is validated by comparing the signals from various uncorrelated signals. First, signals from the eight independent Direct Current Current Transducers (DCCTs) of the main dipole power converters are collected [36, 37]. The DCCTs measure the converter output current with a sampling rate of 1 kHz. The sum of 50 Hz harmonics is also observed in their spectra with a similar frequency modulation. For the analysis of the DCCT signals, the fundamental harmonic (h=1) is selected. An accurate determination of the modulation directly at 50 Hz requires a more refined Fourier analysis to overcome the problem of limited resolution. For this reason, the Numerical Analysis and Fundamental Frequencies (NAFF) algorithm is employed [38, 39]. The green curve of Fig. 7 presents the frequency evolution of the 50 Hz line, as observed in the DCCTs. All eight independent measurements reveal an oscillation which is synchronous in phase and equal in amplitude. The origin of this common drift, which is observed both in the eight DCCTs and the beam, is the stability of the 50 Hz mains from the power grid. This conclusion can also be verified by comparing the drift with unrelated signals acquired from other machines of the accelerator complex, such as the SPS, where the measured drift was identical to the one observed in the LHC signals.

To further support this conclusion, the beam spectrum is compared to the output voltage spectrum of the Main Bends power converter installed in sector 1-2. During the MD Fill 7343, voltage measurements of the power converter were collected every minute with a sampling rate of 50 kHz. The converter's spectrum consists of 50 Hz harmonics, extending up to 10 kHz. Figure 8 illustrates the voltage spectrogram for a regime in the low (left) and high (right) frequency cluster. Applying a similar analysis to the one used for the harmonics of the beam yields

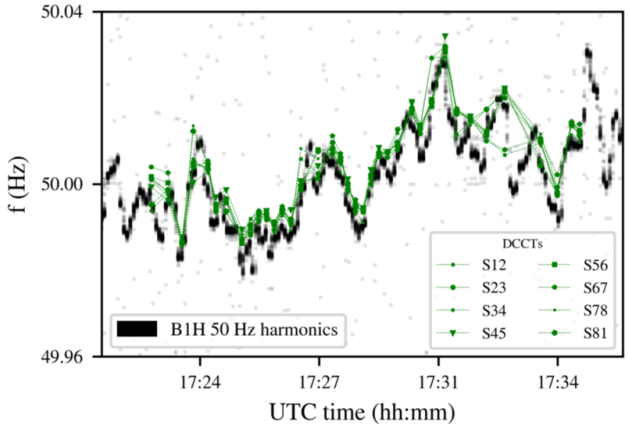

FIG. 7. The frequency modulation of the harmonics observed in the eight DCCTs (green) and the ones of the beam spectrum (black).

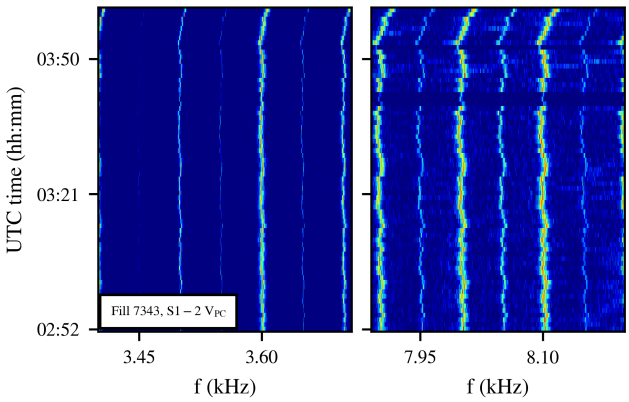

FIG. 8. The voltage spectrum of the power converter of the Main Bends in sector 1-2 for the low (left) and high (right) frequency ranges.

an identical frequency evolution of the 50 Hz components in the power converter. Figure 9 presents the modulation of the lines in the power converter (blue) and the beam (black) for the same time interval, after normalizing with the harmonic order. The strong correlation between the two enhances the hypothesis that the modulation originates from the stability of the mains. It is interesting to note that, at the end of the MD (6 am Central European Time), a frequency drift above the usual variation of the 50 Hz is visible in both spectra. To validate that this effect is reproducible, fills for the same time and different days have been analyzed, yielding similar results. These variations appear to be the result of the changing load of the power grid at this time of the day.

The previous findings are not meant to establish a correlation between the dipole power converter in sector 1-2 and the beam. The importance of these observations resides on the fact that, if the 50 Hz harmonics are the

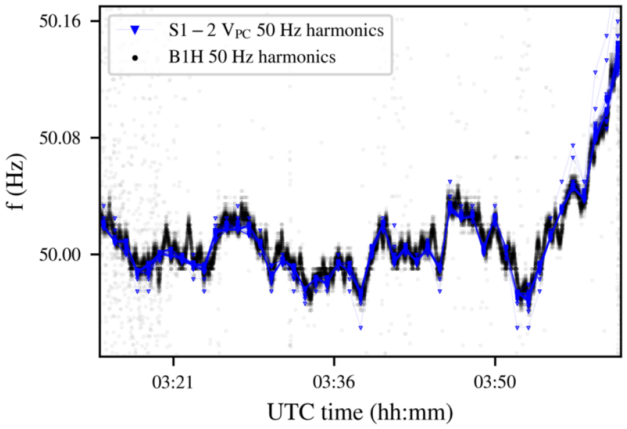

FIG. 9. The frequency modulation of the harmonics observed in the voltage spectrum of the main dipoles power converter of sector 1-2 (blue) and the ones of the beam spectrum (black).

results of a real beam excitation, their frequency domain signature points to a specific type of power converter as the noise source. In particular, the existence of multiple 50 Hz harmonics in combination with the frequency modulation induced by the mains suggests that the origin of these frequency lines are power converters that are based on commutated Thyristor Technology. This can be understood with a frequency analysis of the variation of the magnetic field (B-Train) in two other machines of the accelerator complex: the Proton Synchrotron (PS) and the and SPS [40, 41]. In the B-Train system, a pickup up coil is installed in the aperture of the reference dipole magnets. The measured signals correspond to the rate of change of the magnetic field. Figure 10 shows the spectrogram of the magnetic measurements for the PS (Fig. 10a) and SPS (Fig. 10b). The PS spectrum reveals a strong component at 5 kHz, which is the frequency of some of its Switch-Mode power converters [42]. The switching of this type of power converter is regulated by a clock. Subsequently, a negligible variation in the frequency evolution of the line is observed. As the switching frequencies are well defined, they can be easily identified and no 50 Hz harmonics are present in the signal. On the contrary, in the SPS case, the power converter is a Silicon Controlled Rectifier (SCR). Hence, the 50 Hz harmonics are visible on the signal and the stability of the mains has an impact on the output current of the power converters. In the following studies, when the expected position of the 50 Hz harmonics is illustrated, the drift of the harmonics due to the modulation is taken into account.

Therefore, if environmental noise is excluded as the origin of the perturbation, the signature of the 50 Hz harmonics in the beam spectrum suggests that the possible sources are limited to magnets with SCR power converters. The magnets with such types of power converters in the LHC are presented in Table I [36, 43].

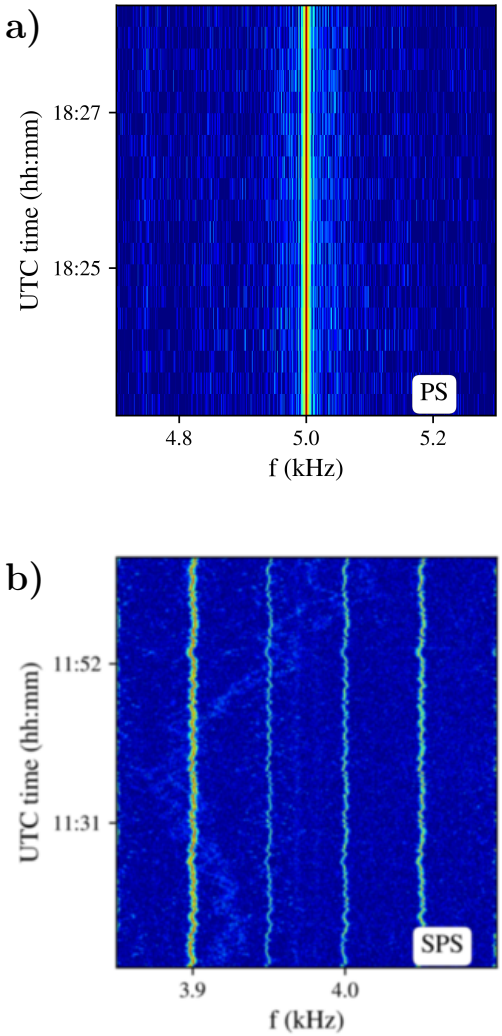

FIG. 10. The spectrum of the B-Train in (a) PS and (b) SPS.

The phase evolution of the 50 Hz harmonics between two locations in the ring can clarify whether the noise lines are the result of a real beam excitation. To this end, their phase advance is measured between two closely separated pickups and is then compared to the betatron phase advance between the same pickups. For the validity of the comparison, the two observation points must be situated in a relatively close distance, so that the beam does not encounter a noise perturbation while crossing this path. If the harmonics are the result of a spurious signal entering the beam then their phase advance is not expected to correspond to the betatronic one. Furthermore, in general, an arbitrary dephasing between the low and high-frequency cluster should be observed. On the contrary, in the case of a real excitation, the noise phase advance must correspond to the betatronic one for all the harmonics present in the spectrum.

In the context of this investigation, two pickups of the transverse damper, referred to as Q7 and Q9, are selected for the analysis. At collision energy, the betatron phase advance between the two observation points is defined by the optics and is approximately equal to 110°. The first step is to compute the complex Fourier spectra for a single pickup and for each bunch in a physics fill to observe the dephasing of the lines across the full machine. As previously reported, with the present noise floor, the evolution of the lines cannot be determined with a single bunch. For this reason, the average signal is computed from five consecutive LHC trains, each one of which consists of 48 bunches. Then, the phase evolution of each harmonic is computed across the accelerator.

TABLE I. The SCR power converters in the LHC [36, 43].

Power converter type	Use
RPTE	Main dipoles
RPTF	Warm quadrupoles (Q4, Q5)
RPTG	Dogleg dipoles (D1, D3, D4, spare)
RPTL	Alice compensator
RPTM	Septa
RPTI	Alice and LHCb dipoles
RPTN	LHCb compensator
RPTJ	CMS Solenoid
RPTH	Alice Solenoid
RPTK	RF Klystron

Figure 11 depicts the dephasing of a harmonic in the low (Fig. 11a) and high-frequency cluster (Fig. 11b) as a function of the train number for Q7 (blue) and Q9 (green). The gray dashed lines illustrate the expected dephasing, which is proportional to the frequency and the time delay of the trailing trains from the first train in the machine. It must be noted that by averaging over a few consecutive trains the signal is sub-sampled to f_{rev}, similarly to the single bunch case. Based on the above, the negative slope of the 7.8 kHz (h=156) shows that the phase evolution of the harmonic was computed through aliasing, i.e., by following the phase evolution of the reflected frequency component around the revolution frequency ($f_{\mathrm{rev}} - 7.8$ kHz). The phase advance of each harmonic is the difference in the phase determination of the two pickups. In both cases, a correspondence to the betatron phase advance is found, an observation that clearly proves, for the first time, that the two harmonics correspond to a real beam excitation.

The filling scheme of the physics Fill 7334 is divided in three groups of consecutive trains. Each group corresponds to approximately one-third of the total beam. The average value and the standard deviation of the dephasing between Q7 and Q9 are computed from the three groups for all the harmonics above noise level. Figure 12 demonstrates the average phase advance for the harmonics in the low (blue) and high (orange) frequency cluster. The error bars represent one standard deviation since following the frequency drift of lower-amplitude harmonics can introduce uncertainties. The gray dashed line in-

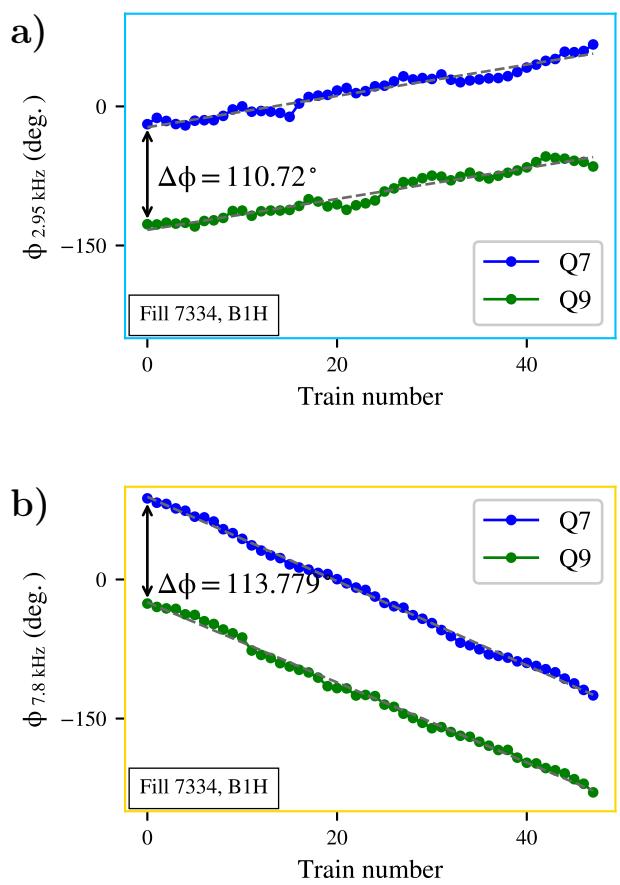

FIG. 11. The phase evolution of the (a) h=59 and (b) h=156 harmonic as a function of the train number for Q7 (blue) and Q9 (green).

dicates the betatron phase advance. The average value demonstrates that, within an uncertainty represented by the standard deviation, the phase advance for all the harmonics is the one of the beam, thus proving that the observations are not instrumental.

C. Observations during changes in the beam and machine configuration

The conclusions of the previous section are based on parasitic observations with a static beam and machine configuration. These findings are further extended with observations acquired during changes in the operational conditions. These modifications refer to, first, the change of the betatron tune and phase advance and second, the beam energy during the cycle. Then, the study focuses on the beam response during a modification in the power converters and finally, in the settings of the transverse damper.

The response of the harmonics during a simple modification of the betatron motion such as the change of

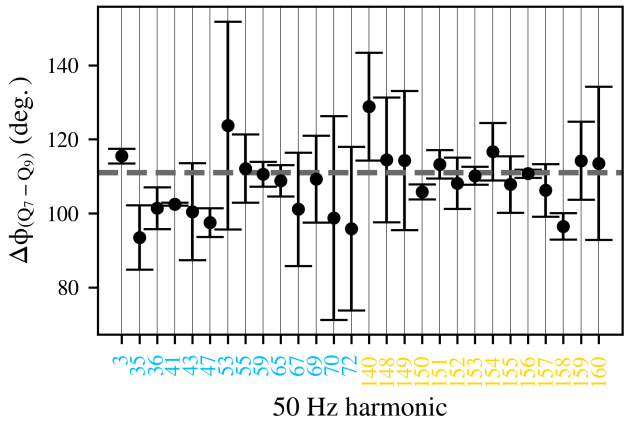

FIG. 12. The average phase advance from Q7 to Q9 for the harmonics in the low (blue) and high (orange) frequency cluster. The error bars represent one standard deviation and the gray dashed line illustrates the betatron phase advance.

the tune at Flat Top is investigated. As previously mentioned, at this point in the cycle, the beam energy reaches the maximum value of 6.5 TeV and, after a few minutes at top energy, the decimal part of the horizontal tune is trimmed from approximately 0.28 to 0.31. Figure 13 presents the HS BBQ spectrogram for the horizontal plane of Beam 1 in the physics Fill 7056. The spectrogram is centered around the betatron tune for the whole duration of Flat Top and a color code is assigned to the PSD. The black dashed line represents an approximation of the horizontal tune evolution. First, one must observe that the frequencies of the lines are not affected by the tune change. This fact proves that the harmonics are the result of a dipolar field error rather than a tune modulation [44]. Second, a comparison prior and after the trim leads to the conclusion that the amplitude of the lines in the vicinity of the betatron tune is strongly enhanced. This resonant behavior is in agreement with a dipolar perturbation, with an excitation frequency that approaches the betatron tune (see Appendix C).

Of particular interest is the impact of the tune change on the high-frequency regime. To investigate this effect, the high bandwidth spectrum is computed from the ADTObsBox prior and after the tune trim. Figure 14 shows the horizontal spectrum of Beam 2 up to 10 kHz (Fig. 14a) at top energy with the injection (blue) and collision (black) tune. Similar observations exist for both beams and planes. Similarly to the HS BBQ, the closest harmonics to the tune of the low-frequency cluster are enhanced in terms of amplitude. It must be noted however, that a shift is also observed at the position of the high-frequency cluster. To further illustrate this effect, the spectrum is centered around the high-frequency cluster in Fig. 14b. Although the effect is dipolar in both cases (the harmonics coincide with the 50 Hz multiples indicated with the gray lines), this observation shows that, as stated in Section II B, the location of the cluster is at

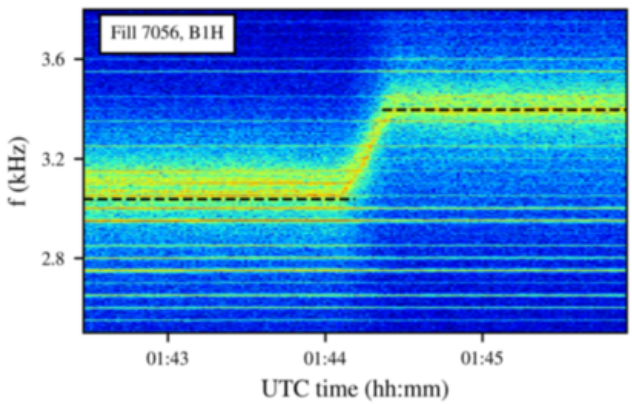

FIG. 13. The horizontal spectrogram of Beam 1 at Flat Top. The black dashed lines represent an approximation of the injection and the collision tune.

$f_{\text{rev}} - f_x$ and thus, depends on the tune. The fact that the changes in the beam configuration affect the amplitude of the noise lines provides further proof that the harmonics are the result of a real beam excitation.

To complement these findings, the response of the harmonics is studied when another modification is applied to the betatron motion and specifically, to its phase advance, while the tune is constant. During the MD Fill 6984, the betatron phase advance between the IP 1 and 5 were modified [45]. This was achieved through the incorporation of a set of optics knobs, which allow scanning the phase between the two IPs, based on the ATS scheme [23]. In this case, the knobs lead to a trim in the current of the quadrupole families responsible for the control of the tune. Throughout these modifications, the betatron tune is constant.

To demonstrate the impact of the knob, Fig. 15 illustrates the converter current for a single quadrupole (red). The evolution of the current corresponds to a change of the phase advance within a range of $\pm$ 20° for the horizontal plane of Beam 1. During this time interval, the amplitude evolution of the harmonics is computed. Figure 15 also denotes the response of the h=12 harmonic (black curve). The amplitude evolution of the lines in the low-frequency cluster is clearly impacted by the variation of the betatron phase advance, an effect that provides definitive indications that they originate from the beam. As far as the high-frequency cluster is concerned, no impact is observed in their amplitude evolution throughout these tests, an effect which is explained later in this paper.

Following the change of the betatron tune and phase advance, we explore the evolution of the spectrum across different beams modes and thereby, different energies and optics. Some of the magnets in Table I can be excluded as potential noise sources by observing the evolution of the spectrum across the cycle. For this reason, the horizontal spectrum of Beam 2 is computed for various beam modes

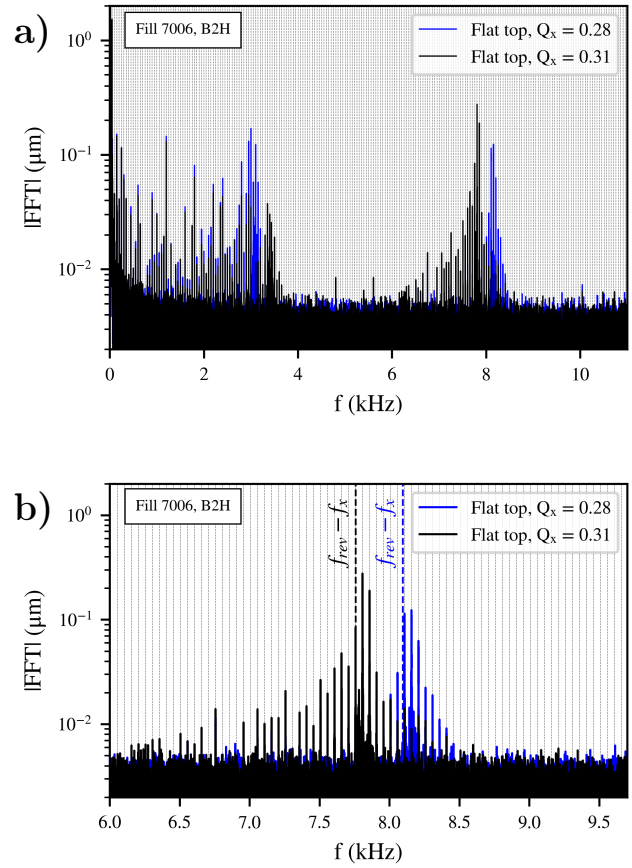

FIG. 14. The horizontal spectrum of Beam 2 prior (blue) and after (black) the tune change (a) at Flat Top and (b) centered around the high-frequency cluster. The gray dashed lines represent the multiples of 50 Hz.

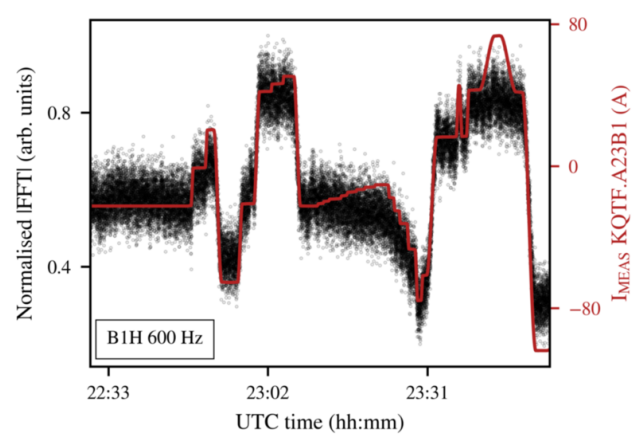

FIG. 15. The amplitude evolution of the 600 Hz lines (black) during the change of the phase advance between IP1 and IP5. while the tune is kept constant. The red line represents the current in the quadrupole trims employed for the phase scan.

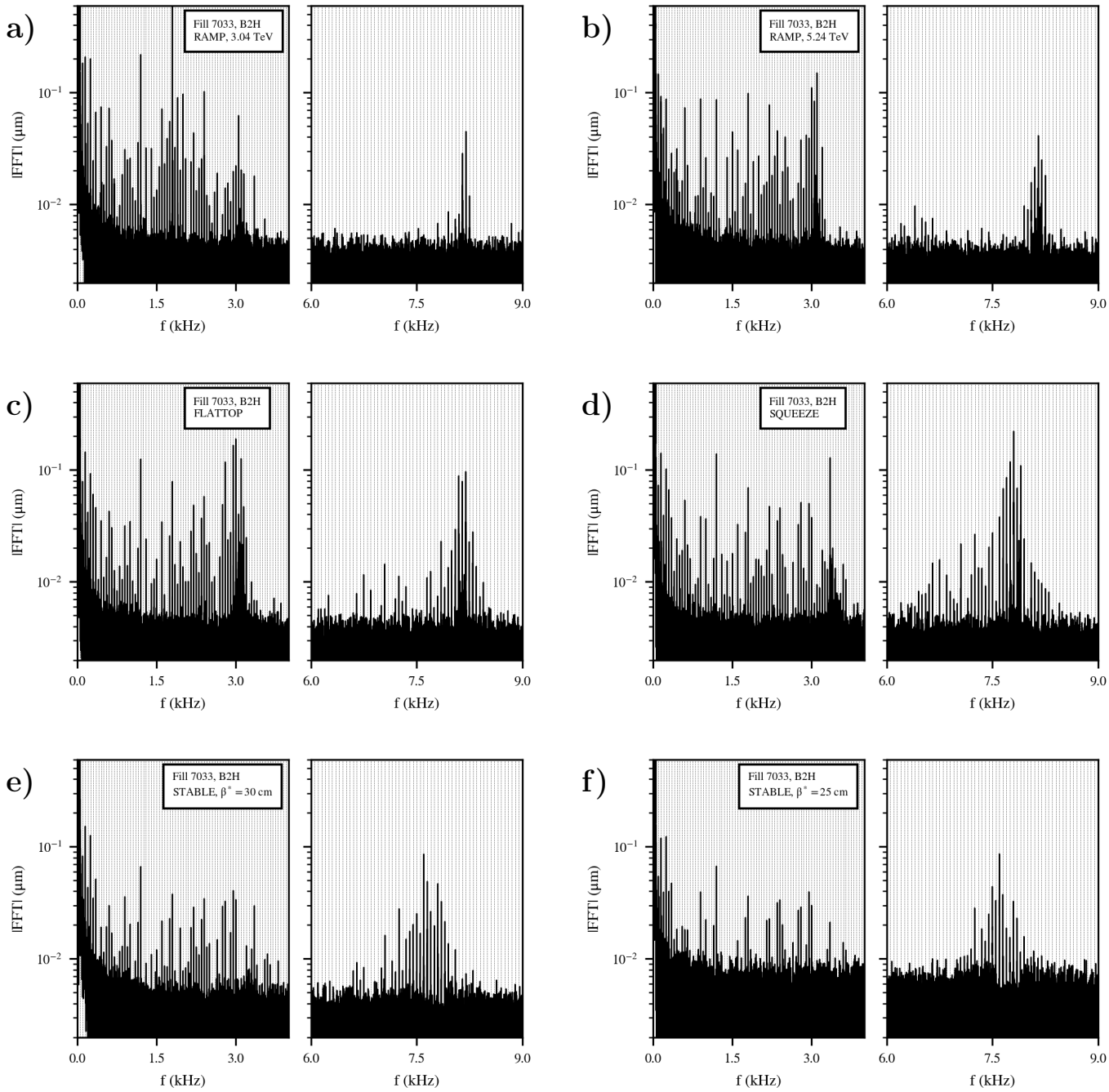

FIG. 16. The horizontal beam spectrum of Beam 2 during Ramp (a,b), Flat Top (c), Squeeze (d) and Stable Beams (e,f).

(physics Fill 7033). For the comparison, we profit from the calibrated metric provided by the ADTObsBox. Figure 16 depicts the spectra, centered around the low (left) and high (right) frequency clusters. The beam modes of particular interest are Ramp (Fig. 16a and 16b) for two values of the energy, Flat Top prior to the change of tune (Fig. 16c), Squeeze (Fig. 16d) and Stable Beams (Fig. 16e and 16f) for two steps of the β^*-leveling.

First, due to the fact that the 50 Hz harmonics are systematically present in all beam modes and fills, the power converters of the spare magnets and the septa are excluded. Second, the amplitude of the noise lines does not significantly attenuate with increasing beam energy. Considering a non-ramping power converter as the source, a reduction of the angular deflection and thus, of the amplitude of the noise, should be observed with increasing beam rigidity. The absence of such an attenuation leads to the conclusion that the noise is originating

from a ramping power converter. Consequently, all non-ramping power converters can also be excluded. Through this process of elimination, the remaining candidates of Table I are the main dipoles and the warm quadrupoles. Combining this finding with previous indications of the dipolar nature of the source, the investigation focuses on the power converters of the Main Bends. The main dipoles have undoubtedly the highest filling coefficient in the ring and, as previously mentioned, the studies conducted in other synchrotrons have proved that the arc circuit was systematically the dominant contributor.

Additionally, reviewing the spectrum at Ramp and Flat top yields a further excitation of the high-frequency cluster across the two beam modes. A comparison between Flat top (injection tune) and Squeeze (collision tune) illustrates the dependence of the position of the high-frequency cluster to the betatron tune, as previously discussed. Finally, the β^* reduction from 30 cm to 25 cm at Stable beams does not have an impact on the amplitude of the harmonics. The increase of the noise floor between the two spectra is due to the reduction of the beam intensity across the two observations.

Based on the previous findings, the pursued investigations focus on the main dipoles circuit. To establish a correlation between the harmonics of the beam and the ones in the output of their power converters, a modification in the configuration of the latter is needed. In this context, an important observation was made when the status of the active filters of the Main Bends, which are installed for the attenuation of the 50 Hz ripples [46–48], was changed. During dedicated MD fills, the eight active filters were disabled sector-by-sector. The main observable throughout these tests is the amplitude evolution of the harmonics. First, the impact on one noise line is demonstrated and then the observations are extended to different beam energies and various harmonics.

Figure 17 depicts the 3D spectrogram for the horizontal plane of Beam 1, as acquired from the MIM, for the time interval of the tests conducted at injection (Fill 7343). For a first demonstration, the frequency range is limited around 600 Hz. The projection of the spectrogram, which represents the amplitude evolution of the h=12 harmonic, is shown with the blue curve. Disabling the eight filters leads to abrupt changes in its amplitude evolution.

To clearly illustrate these results, the amplitude evolution of the h=12 harmonic is extracted from the 3D spectrogram. Figure 18 (top) presents the response of the 600 Hz line in Beam 1 (blue) and 2 (red) for two separate beam modes: a fill at injection (Fig. 18a) and at top energy (Fig. 18b). The status of the eight active filters is presented for the same time span (bottom) and a color code is assigned to each sector. The distinct changes in the amplitude coincide with the disabling of the filter of each sector. As a last step at injection, the filters were disabled simultaneously, which led to an important increase in the amplitude of the line.

The observations on the h=12 harmonic provide evidence that all eight power converters contribute to this effect. The question that arises is whether the most impacted sectors in terms of noise can be identified. Reviewing the results of Fig. 18 yields that the positive or negative impact of the filter compared to the baseline, which is defined as the amplitude of the harmonic prior to the test, depends on the sector. For instance, at injection in Beam 1, disabling the Filter of sector 1-2 leads to an increase of the ripple amplitude. Therefore, the filter, when active, suppresses the harmonic and its impact is characterized as positive. On the contrary, sector 5-6 has a negative contribution at injection. Then, comparing the same sector across the two beams reveals a different impact between the two (e.g., sector 5-6 at injection). This can be possibly attributed to the different phase advance of the two beams in the ring. Finally, the contribution for the same beam and sector also depends on the beam energy (e.g., Beam 2, sector 3-4).

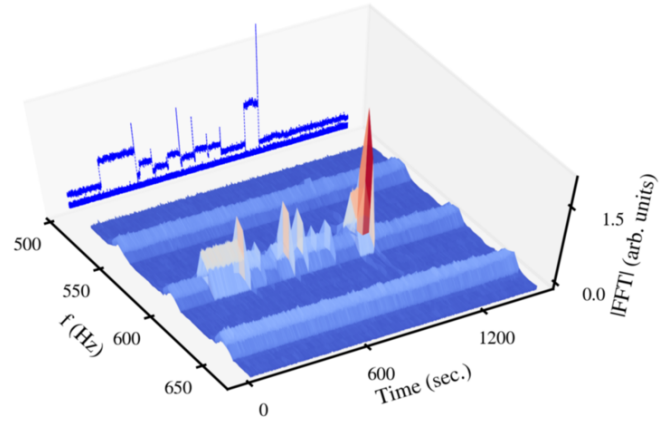

FIG. 17. The horizontal spectrogram of Beam 1 during the tests of the active filters at injection centered around 600 Hz. The blue lines represent the amplitude evolution of the spectral components in this regime.

The correlation with the power converters is not only valid for the 600 Hz line, but for most of the 50 Hz harmonics included in the low-frequency cluster. Figure 19 shows the amplitude evolution of various harmonics at injection, represented with a different color code. The abrupt changes in the amplitude when disabling the active filter of each sector are reproduced for harmonics up to 3.6 kHz. In addition to the observations at 600 Hz, the contribution of each sector also varies across the harmonics.

To summarize, applying a simple modification in the configuration of the dipole power converters, such as modifying the status of the active filters, has a direct impact on the low-frequency cluster harmonics of the beam. These results provide evidence that the power converters of the main dipoles are at least a major contributor to the harmonics up to 3.6 kHz observed in the beam spectrum. It is the first time that such a correlation has been demonstrated in the LHC. Presently, the transfer function from the active filters to the transverse beam

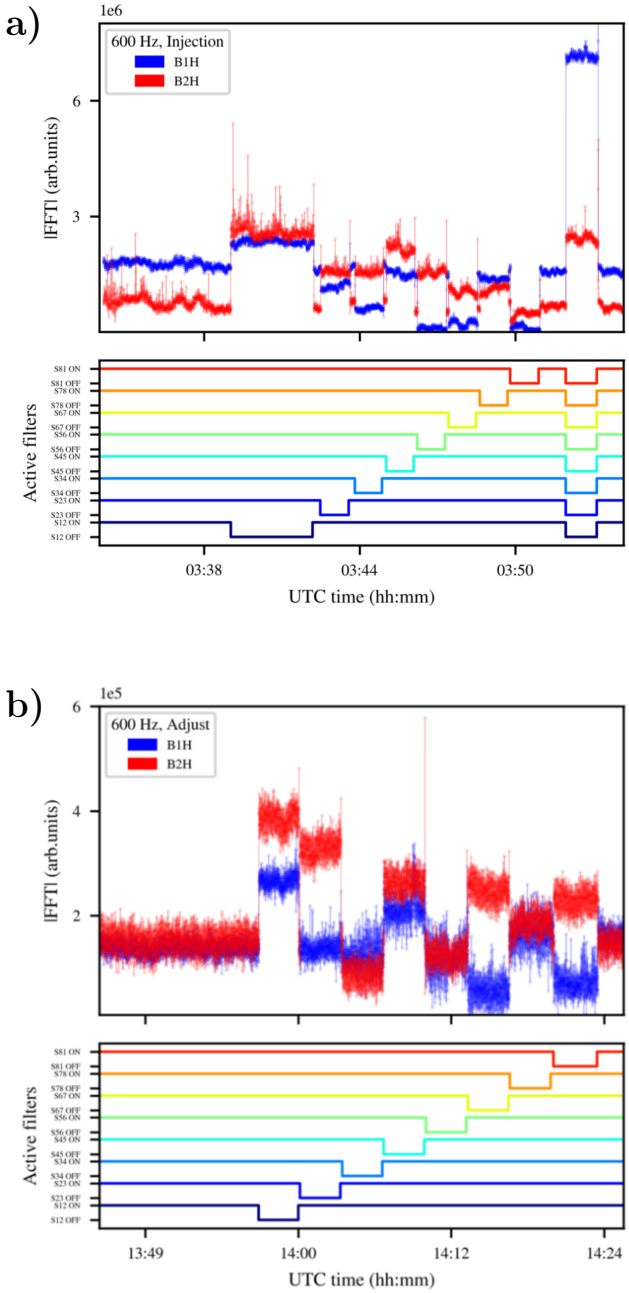

FIG. 18. The response of the h=12 harmonic (top) during the tests with the active filters for Beam 1 (blue) and Beam 2 (red) (a) at injection and (b) top energy. The status of the active filters is color-coded with the sector number (bottom).

spectra, as a function of the sector, the beam energy and the order of the harmonic is not known and therefore, a classification of the sectors in terms of noise is not currently performed.

It must also be underlined that no change in the amplitude evolution of the harmonics in the high-frequency cluster is reported during these tests. Figure 20 demonstrates the voltage spectrum of the power converter in one

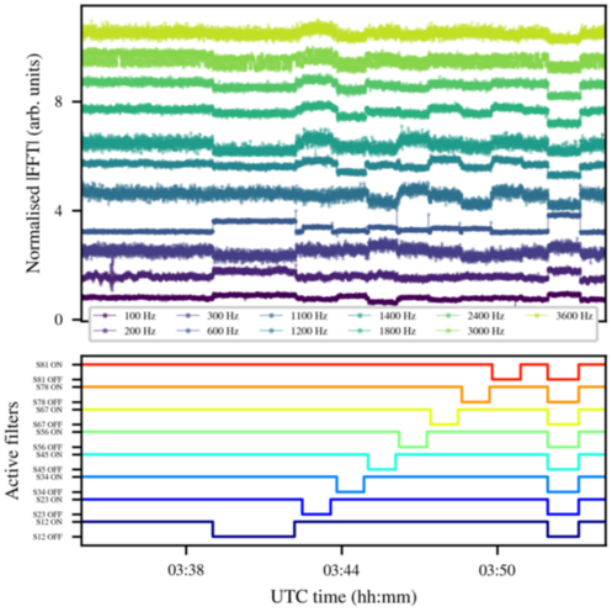

FIG. 19. The amplitude evolution of the harmonics in the low-frequency cluster (up to 3.6 kHz) during the tests with the active filters.

of the LHC sectors, first, when the active filter is enabled (Fig. 20a) and, then, disabled (Fig. 20b). In this case, the vertical lines represent the multiples of 600 Hz. The comparison of the spectrum prior and after the modification shows that the active filter is suppressing some of the harmonics up to approximately 3 kHz, while it enhances the high-order harmonics [48]. However, the amplitude of the high-frequency cluster in the beam spectrum did not increase during these tests, an effect which is explained later in the present paper.

A comparison between the spectra of the horizontal and vertical plane provides yet another indication of the dipolar nature of the source. The spectra of both beams and planes are measured for the physics Fill 7334. As the pickups for the two beams and planes are located in different positions in the ring, the ADTObsBox calibrated spectra are normalized with the corresponding β-functions (see Appendix C). Figure 21 demonstrates the spectra for the horizontal (magenta) and vertical (cyan) plane for Beam 1 (left) and 2 (right). Comparing the amplitudes of the spectral lines yields that the perturbation is mainly affecting the horizontal plane, an effect compatible with a dipolar field error. Due to the transverse coupling of the machine, an attenuated perturbation is also present in the vertical plane. To demonstrate that this effect results from the coupling, controlled excitations have been applied in the horizontal plane of Beam 1 using the transverse damper in a dedicated MD fill (see Appendix D). In this case, although only the horizontal plane was excited, the oscillation was visible also in the vertical plane.

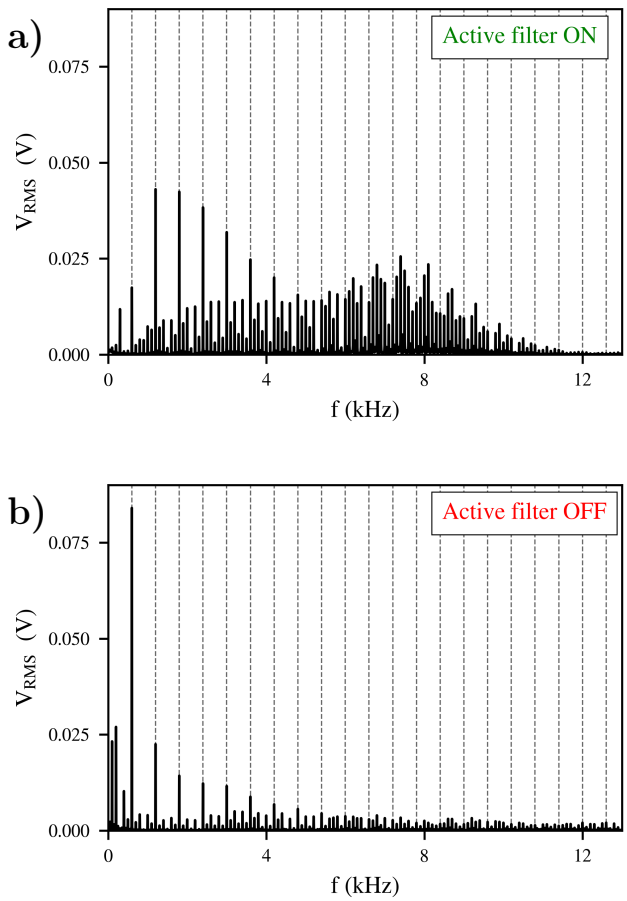

FIG. 20. Voltage spectrum of the power converter of the main dipoles in one of the LHC arcs (Sector 1-2) with the active filter (a) enabled and (b) disabled. The vertical gray lines represent the multiples of 600 Hz.

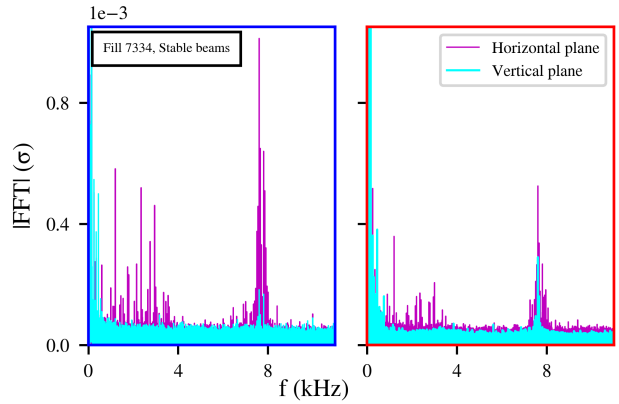

FIG. 21. The spectrum of the horizontal (magenta) and vertical (cyan) plane of Beam 1 (blue) and 2 (red) in Stable Beams, normalized with the corresponding β-functions.

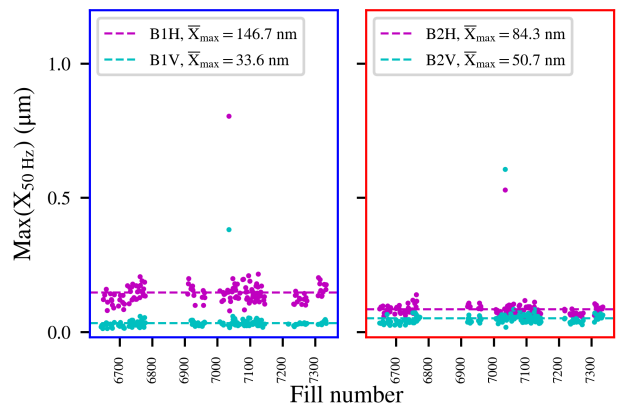

FIG. 22. The maximum amplitude of the 50 Hz harmonics for the horizontal (magenta) and vertical plane (cyan) of Beam 1 (blue) and 2 (red) for all the proton physics fills of 2018.

Furthermore, it must be highlighted that the maximum offset observed in the horizontal spectrum of Beam 1 is approximately 0.1 μm, which corresponds to 10^{-3} σ. As shown in Appendix C, assuming a single dipolar perturbation, this value corresponds to a deflection of 0.09 nrad at a location with $\beta = 105$ m for an excitation frequency in the vicinity of the tune. Comparing the equivalent kick with the bending angle of a single dipole in the LHC ($\approx$5 mrad) and neglecting additional effects (transverse damper, electron-cloud, transverse impedance) yields a field stability of $1.8 \cdot 10^{-8}$, a value which is well within the power converter specifications.

Comparing the spectra of the two beams yields an asymmetry in terms of noise between Beam 1 and 2. Based on the amplitudes of the spectral components, a more significant effect is visible in Beam 1. To verify the reproducibility of this observation, the spectra of both beams and planes are computed for all the proton physics fills of 2018. For each fill, the maximum offset induced by the 50 Hz harmonics is computed, which corresponds, in Stable Beams, to a frequency of 7.7 kHz. Figure 22 depicts the maximum amplitude observed in the spectrum as a function of the fill number for the horizontal (magenta) and vertical (cyan) plane in Beam 1 (blue) and 2 (red). The dashed lines represent the average offset over all the fills for each plane. These results confirm that the noise is systematically more pronounced in Beam 1 than Beam 2 by approximately a factor of two in the horizontal plane.

The fill-by-fill analysis of the spectra reveals an increase of the noise in terms of amplitude in the physics Fill 7035. In this context, an additional parameter that has not been included in the analysis so far is the activity of the transverse damper and the interplay with the 50 Hz harmonics. In the nominal LHC cycle, the ADT settings are modified and in particular, the extended ADT bandwidth is changed to standard bandwidth at the end of Adjust [49, 50]. In the Fill 7035, this modification was not applied and the extended bandwidth was used at Stable Beams. Figure 23 illustrates the horizontal

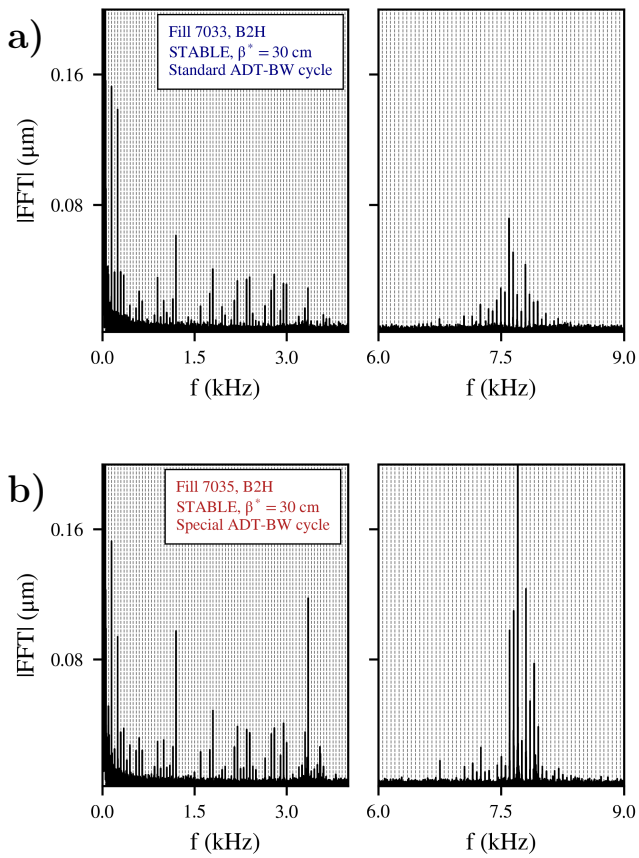

FIG. 23. The horizontal spectrum of Beam 2 at Stable Beams centered around the low (left) and high (right) frequency cluster for a fill with (a) the standard (Fill 7033) and (b) extended (Fill 7035) ADT bandwidth.

spectrum of Beam 2 at Stable Beams for the Fill 7033 (Fig. 23a) with the standard ADT bandwidth and for the Fill 7035 (Fig. 23b). Comparing the two spectra yields an increase in the amplitude of the 50 Hz harmonics in the regime above 3 kHz, which is particularly important for the high-frequency cluster. This observation indicates that the high-order harmonics are suppressed by the damper in normal operation. This also explains why an amplitude increase of the high-frequency cluster was not observed when the corresponding harmonics in the power converter's voltage spectrum increased during the active filters tests. The impact of the ADT settings is also systematically observed in other beam modes of the machine cycle during which the bandwidth was modified such as the Adjust.

The importance of this finding resides on the fact that a strong asymmetry is present between the frequencies of the low and high cluster in terms of amplitude. In particular, these observations indicate that, in the absence of the damper, the amplitude of the harmonics in the high-frequency cluster is expected to be further enhanced compared to the values that have been observed experimentally. In contrast, Fig. 20a shows that the noise

TABLE II. The summary of the observations for the low and high-frequency cluster.

low-frequency cluster[a]	high-frequency cluster[b]
Presence of 50 Hz	
Frequency modulation from the mains	
Phase advance Q7-Q9 compatible with betatronic	
Dipolar nature	
Mainly in the horizontal plane	
Higher amplitude in Beam 1	
Impact from IP1/5 phase scan	Impact from change of tune
Impact from active filters	Impact from ADT settings

[a] Extending up to 3.6 kHz.
[b] Located at 7-8 kHz, depending on the tune.

in the power converter voltage spectrum attenuates with increasing frequency. Although the active filters enhance the high-order harmonics in the power converter voltage spectrum, their amplitude is still lower than the ones of the low-order harmonics. Furthermore, high-frequency perturbations such as the high-frequency cluster strongly exceed the cutoff frequency of the LHC main dipoles due to the shielding effect of the beam screen [51]. To this end, if the high-frequency cluster is driven by a direct excitation due to power converter noise, a significant attenuation of its amplitude should be observed compared to the low-frequency cluster, while experimentally we observed the opposite.

Additionally, it should be mentioned that the increase of the noise by a factor of two in Fill 7035 did not lead to an increase of losses or emittance growth compared to the rest of the fills. However, as the duration of the fill was limited to 40 minutes, the impact of the noise lines on the beam lifetime cannot be excluded.

D. Summary of observations and discussion

The beam transverse spectra, as computed from the ADTObsBox bunch-by-bunch acquisitions, reveal the existence of 50 Hz harmonic perturbations in two frequency regimes, referred to as the low and high-frequency cluster. Although many similarities have been identified between the low and high-frequency cluster, the need to distinguish the two regimes is justified by their different response when modifications in the machine configuration are applied. Comparing the amplitudes of the noise lines residing in each regime yields that larger excitation amplitudes are observed on the beam motion due to the high-frequency cluster. This section summarizes the findings, organizes the observations per cluster, discusses possible sources and presents the conclusions from the experimental observations. A summary of the most important findings can be found in Table II.

The analysis in frequency domain illustrates a common signature between the two clusters. Both regimes

consist of a set of 50 Hz harmonics, that experience a frequency modulation induced by the mains. Several observations prove that both regimes are the result of a real beam excitation. Based on the fact that the harmonics are multiples of 50 Hz rather than sidebands around the tune, and that the horizontal plane is mainly affected, it is concluded that the nature of the source is dipolar. The signature of the harmonics in both regimes is compatible with a ramping SCR power converter. Comparing the spectra of the two beams shows that a larger impact is systematically observed in Beam 1 across all proton physics fills in 2018.

For the low-frequency cluster, it is reported that changing the betatron phase advance between IP1 and 5 had an impact on the amplitude evolution of these harmonics, which further proves that they are coupled to the beam. A correlation with the power converters of the main dipoles has been demonstrated. The status of the active filters has an impact on their amplitude evolution, an effect which proves that all eight sectors contribute to this effect. The response of the lines depends on the beam energy, the beam that is considered and the order of the harmonic. A model to quantify the beam response to each sector cannot be determined at the moment. From these experiments, it is concluded that the 50 Hz harmonics extending up to 3.6 kHz are the result of a direct excitation due to noise in the LHC main dipoles.

The amplitude of the beam oscillations in the high-frequency cluster is larger if compared to the low-frequency cluster, hence the importance to identify its origin. If both clusters emerge from a common source, the question that arises is what is the mechanism that allows these high-frequency components to excite the beam. In fact, oscillations at such high frequencies are expected to be significantly attenuated by the shielding effect of the beam screen in the dipole magnets [51]. A review of the power converter's spectrum in sector 1-2 (Fig. 20)reveals that there is a reduction of the noise with increasing frequency. To this end, the impact of the harmonics above 3.6 kHz was expected to be negligible compared to the low-frequency cluster. On the contrary, experimental observations indicate the presence of important spectral components in the frequency regime of $f_{\mathrm{rev}} - f_x$. More interestingly, the amplitude increase of the lines when the ADT settings are modified indicates that, in normal operation, the high-frequency cluster is suppressed by the damper. This fact underlines that, in the absence of the damper, there is a significant asymmetry between the two clusters in terms of amplitude as the high-frequency cluster is expected to be even further enhanced. An additional observation is that there is a dependence of the cluster's location on the betatron tune. A resonant behavior of noise lines around f_x and $f_{\mathrm{rev}} - f_x$ is indeed expected from a direct dipolar excitation but it does not explain the higher sensitivity observed around $f_{\mathrm{rev}} - f_x$ compared to f_x. Combining this information suggests that, rather than a direct excitation, the high-frequency cluster is the result of the interplay between noise from the dipoles and a mechanism originating from the beam. In particular, the transfer function from the power converter voltage to the magnetic field seen by the beam indicates that the noise reduces with increasing frequency however, it does not consider the beam response. Therefore, the asymmetry between the two clusters can be explained if there is a higher sensitivity of the beam response in the regime $f_{\mathrm{rev}} - f_x$, leading to important offsets from small noise perturbations. For instance, a potential candidate is the interplay of the beam with the machine transverse impedance, as the first unstable mode is at $f_{\mathrm{rev}} - f_x$ [52]. Further observations and experiments are necessary to verify this hypothesis and to identify the exact mechanism that is responsible for the asymmetry between the two regimes. Finally, it should be mentioned that, regardless of the perturbation source, it has been demonstrated that the transverse damper can effectively suppress these harmonics. To this end, the capabilities of the transverse damper can be employed in the future as a mitigation measure against this noise perturbation, without the need to apply modifications on the power converters.

In the context of these studies, a general framework for the analysis of the experimental data has been developed and presented in the previous sections. These tools include computing high-bandwidth spectra from bunch-by-bunch acquisitions while preserving the signal metric and reducing the noise threshold, as well as methods to determine whether a frequency component in the beam spectrum is the result of a real excitation. The analysis presented in this paper can be used to address other types of noise effects. Following the experimental observations, the next sections are dedicated to simulation studies.

III. SIMULATION BENCHMARK WITH CONTROLLED EXCITATIONS

During the latest LHC run, controlled dipolar excitations were applied on the beam using the transverse damper kicker, in order to study the impact of dipolar noise at various frequencies and amplitudes. These excitations were performed at injection energy for two fills, consisting of a single bunch and three equally spaced trains of 48 bunches, respectively. Such a filling scheme provides a uniform sampling rate for the Fourier analysis of the ADTObsBox data. The aim of this section is to validate our simulation framework in a controlled manner.

Experimentally, some of the excitations led to a significant reduction of the beam lifetime. To retrieve the initial deflection applied from the transverse damper, the offset and the frequency are extracted from the calibrated ADTObsBox beam spectrum. For instance, Fig. 24 shows the horizontal spectrum of Beam 1 (single bunch fill) during a controlled excitation at 2.5 kHz (green star-shaped marker). Then, based on these two parameters, the equivalent kick at the location of one of the ADT

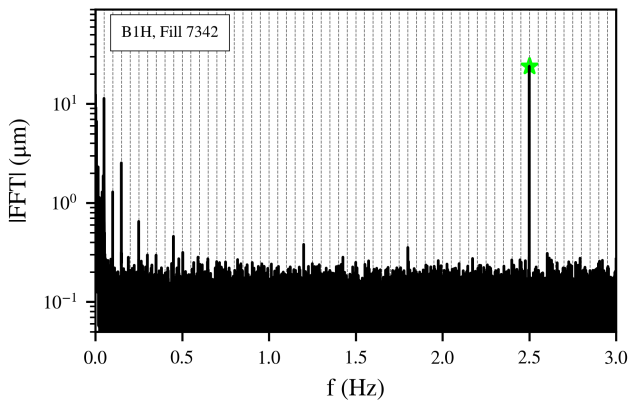

FIG. 24. A controlled dipolar excitation at 2.5 kHz (green marker) in the horizontal spectrum of Beam 1 (black). The vertical lines represent the multiples of 50 Hz.

kickers is computed (see Eq. C6 in Appendix C). This procedure is repeated for all the excitations applied during the tests

The impact of the excitations on the beam lifetime is compared against the DA thresholds computed with tracking studies in the presence of dipolar noise. To this end, simulations are performed with the symplectic single-particle tracking code, SixTrack [53, 54]. In the simulations, a distribution of particles, forming a polar grid in the $x-y$ plane, are tracked for 10^6 turns (≈90 seconds in operation) in the LHC lattice at injection energy and with similar conditions to the experimental setup. The polar grid consists of nine angles and a radius from two to ten σ of initial transverse positions with a step of two σ. The tracking is performed in 6D, i.e., the synchrotron oscillations are also considered and all particles are placed longitudinally at 3/4 of the bucket height. Furthermore, a horizontal modulated dipolar noise source is included at the location of one of the ADT kickers, while the observation point is located at the position of the Q7 pickup. To simulate the dipolar excitation, the strength of a horizontal kicker is modulated with a sinusoidal function. The parameters used in the simulations are presented in Table III. In each study, a different combination of the excitation frequency and amplitude is selected. In particular, considering a constant excitation frequency, the value of the kick is increased and the minimum DA is computed for each case. In this way, a noise amplitude threshold is defined and beyond this limit a reduction of DA is expected. Figure 25 presents the frequency of the excitation as a function of the deflection. A color code is assigned to the minimum DA to distinguish the regime where the noise has no significant impact (blue) from the one where a reduction of DA (red) is anticipated based on the simulations.

In Fig. 25, the star-shaped markers denote the experimental excitation kicks and frequencies. A color code is assigned to the markers that allows distinguishing the excitations that had no impact on lifetime experimentally (blue) from those that lead to a lifetime drop (red). Although an excitation at 8.1 kHz was performed experimentally, the position measurements at this time were not stored and a star-shaped marker is not included. The comparison between experimental observations and the noise threshold defined by DA simulations yields a fairly good agreement between the two for the majority of the excitations, taking into account the simplicity of the machine model and the absence of effects such as linear and non-linear imperfections. This comparison provides a validation of our simulation framework including noise. Additional observations from the controlled excitations such as the coupling of the noise, first, from the horizontal to the vertical plane and, second, between the two beams through long-range beam-beam encounters in the presence of trains are discussed in Appendix D. The method to benchmark simulations and experimental findings presented in this section is not only limited to these studies but can be used to validate the tracking results for different types of noise effects.

TABLE III. The LHC parameters at injection energy used in the simulations with dipolar noise.

Parameters (unit)	Values
Beam energy (GeV)	450
Bunch spacing (ns)	25
R.m.s. bunch length (m)	0.13
RF voltage (MV)	8
Betatron tunes (Q_x, Q_y)	(62.275, 60.295)
Normalized emittance (μm rad)	2.5
Chromaticity	15
Octupole current (A)	20
Bunch population (protons)	1.15e11
Horizontal β at Q7 (m)	130.9
Horizontal β at kick (m)	272.8

IV. SIMULATIONS WITH NOISE

In the following section, the impact of modulated dipolar excitations on the LHC beam performance is discussed in terms of DA, tune diffusion and losses. The simulations are organized as follows. First, a scan in the noise parameter space (f_r, A_r) is performed, where f_r, A_r represent the frequency and the amplitude of the noise, respectively. The aim of this study is to define the most dangerous tones of the low and high-frequency cluster, i.e., the frequencies that, for a constant excitation amplitude, have a maximum impact on the DA. In this context, the minimum amplitude of the excitation that leads to a reduction of DA is determined by considering individual tones. In the presence of multiple harmonics, similarly to the experimental observations, the impact on the beam performance is expected to be more significant. To this end, the offsets of the largest 50 Hz harmonics are extracted from the beam spectrum of a physics fill at

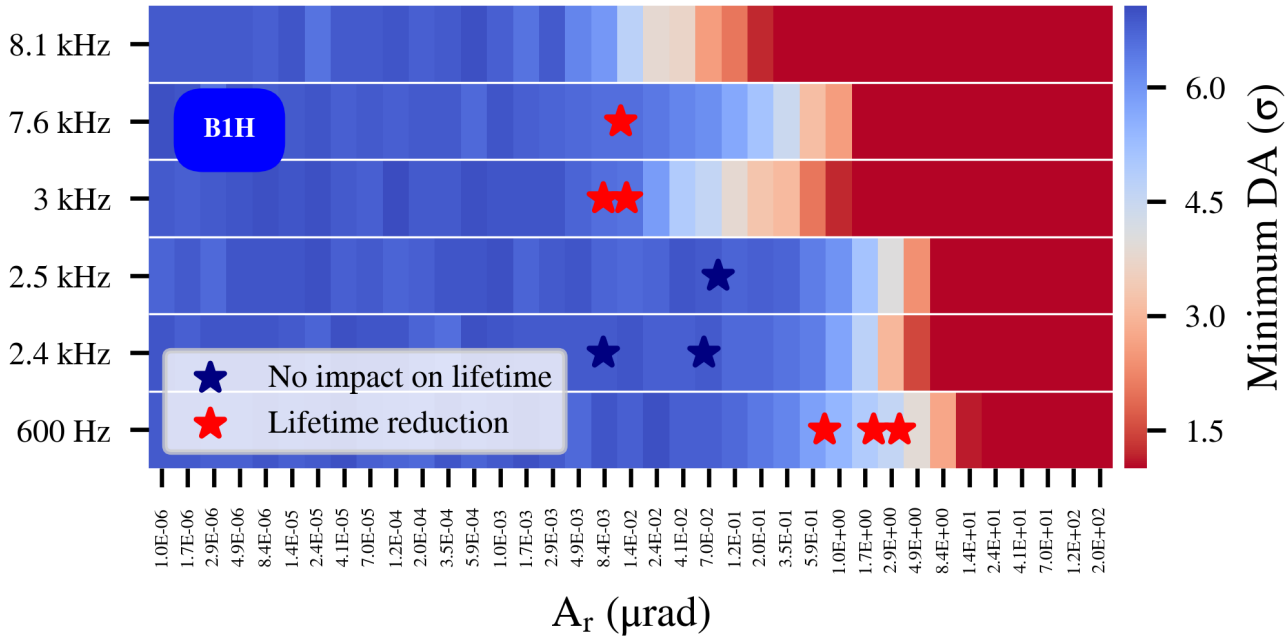

FIG. 25. The frequency of the excitation as a function of the deflection. A color code is assigned to the minimum DA computed with tracking simulations including noise. The star-shaped markers present the equivalent kicks, as computed from the beam spectrum during the controlled ADT excitations. The red and blue markers indicate whether a reduction of lifetime was or was not observed experimentally, respectively.

Stable Beams. In Section II C, it was demonstrated that, as far as the low-frequency cluster is concerned, the noise is distributed in all eight sectors. An accurate representation of the noise propagation across the chains of the LHC dipoles requires a model of the transfer function as a transmission line for all the spectral components in the low-frequency cluster, similarly to the studies performed for the SPS [55]. Furthermore, as the exact mechanism of the high-frequency cluster is not yet identified, an accurate transfer function is not known at the moment. To simplify these studies, a lumped noise model is employed. From the extracted offsets, the equivalent deflections are computed for a specific position in the LHC ring. In this way, the contribution of all the dipoles is represented by a single, equivalent kick and the offsets observed in the LHC spectrum are reproduced in the simulations.

The simulations are then repeated for the HL-LHC case. The need to perform projections for the HL-LHC is justified by the fact that no modifications are envisaged for the power converters of the main dipoles. Consequently, based on the source, the 50 Hz harmonic are expected to also be present in the HL-LHC era. In the following sections, the HL-LHC studies are based on the noise spectrum acquired experimentally from LHC, although the foreseen upgrade of the transverse damper system can lead to a more efficient suppression of the harmonics. The main parameters used in simulations for LHC and HL-LHC are presented in Table IV. The simulated conditions in the HL-LHC case correspond to the nominal operational scenario at the end of the β^*-leveling, taking place a few hours after the start of Stable Beams.

TABLE IV. The LHC and HL-LHC parameters at Stable beams used in the simulations.

Parameters (unit)	LHC	HL-LHC[a]
Beam energy (TeV)	6.5	7
Bunch spacing (ns)	25	25
R.m.s. bunch length (m)	0.075	0.075
Horizontal tune (Q_x)	62.31	62.31/62.315[b]
Vertical tune (Q_y)	60.32/60.315[b]	60.32
Normalized emittance (μm rad)	2.0	2.5
Chromaticity	15	15
Octupole current (A)	550	-300
Bunch population (protons)	1.25e11	1.2e11
IP1/5 Half crossing angle (μrad)	160	250
IP1/5 β^* (cm)	30	15
Horizontal β lumped noise (m)	105.4	102.3

[a] End of β^*-leveling.
[b] Nominal/optimized working point.

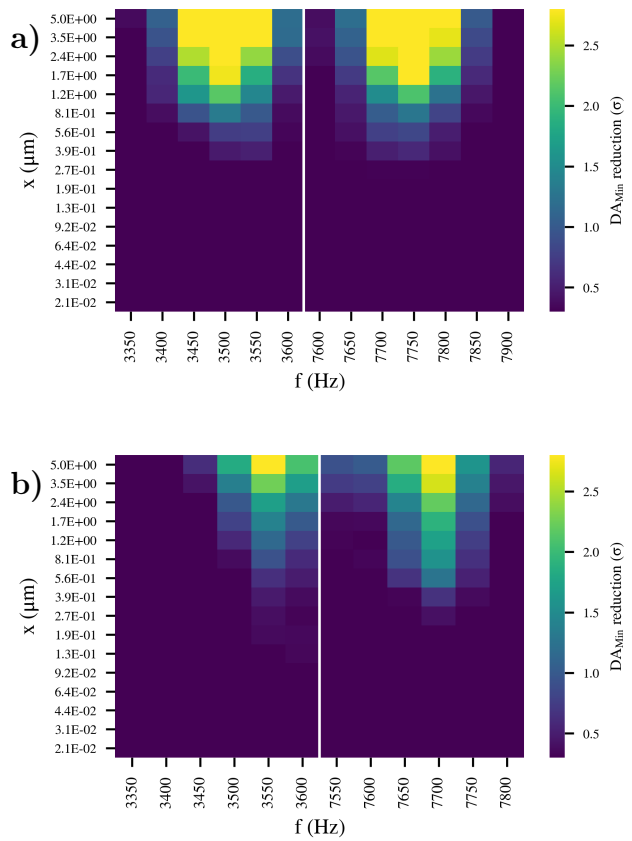

FIG. 26. A scan of individual frequencies as a function of the offset for (a) LHC and (b) HL-LHC. A color code is assigned to the reduction of DA compared to the DA in the absence of noise.

A. Impact of single tones on Dynamic Aperture

Similarly to Section III, the DA simulations are performed for the LHC and HL-LHC lattice at collision energy. For each study, a different combination of the frequency and the amplitude of the excitation is selected. For each case, the minimum DA is compared to the value derived in the absence of noise. Figure 26 presents the results of the frequency scan as a function of the noise-induced offset for LHC (Fig. 26a) and HL-LHC (Fig. 26b). The offset is computed using Eq. (C6) in Appendix C. Specifically, the harmonics of the low and the high-frequency cluster that reside in the vicinity of f_x and $f_{\rm rev} - f_x$ have been selected for the analysis. A color code is assigned to the reduction of the minimum DA. From the scan, it is evident that the most dangerous frequencies are the ones that reside in the proximity of the tune and its alias. For the LHC, an offset threshold of 0.4 μm is defined, while this limit reduces to 0.2 μm for the HL-LHC. For comparison, the maximum excitation observed experimentally due to the 50 Hz lines is approximately 0.1 μm.

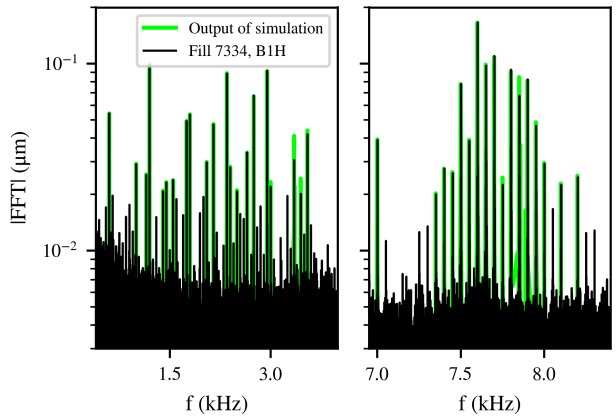

FIG. 27. The spectrum for the low (left) and high (right) frequency clusters as acquired from the horizontal plane of Beam 1 for the physics Fill 7334 (black) and from tracking (green).

B. Frequency Map Analysis with a realistic noise spectrum

From the spectrum of a physics fill (Fill 7334), the offsets of the 40 largest 50 Hz harmonics are extracted. The equivalent kick at the location of the Q7 pickup is computed and used as an input for the noise simulations. Figure 27 shows the spectrum from the experimental observations (black) and the output of the simulations (green) after tracking a single particle at 0.1 σ for the low (left) and high (right) frequency cluster. The comparison of the two is a sanity check illustrating the good agreement between the simulated and the experimental beam spectrum. A similar agreement (between simulated and expected beam spectrum) is found for the HL-LHC case, were the equivalent kicks have been recomputed due to a small variation of the β-functions.

The studies have been organized in the following way: first, a study in the absence of noise is performed which defines the reference conditions. Second, the largest 50 Hz harmonics of the low-frequency cluster are considered. Then, a separate study is conducted including only the most important harmonics of the high-frequency cluster. Last, both regimes are included in the simulations. A Frequency Map Analysis (FMA) is performed for each study [56–59]. Particles forming a polar grid in the configuration space from 0.1 to 6.1 σ with a step of 1 σ and 99 angles are tracked for 10^4 turns in 5D, i.e., without considering the impact of the synchrotron motion. The turn-by-turn data are divided into two groups containing the first and last 2000 turns, respectively. The tune of each particle is computed for each time interval using the NAFF algorithm. Comparing the variation of the tune of each particle across the two time spans reveals information concerning its tune diffusion. For the frequency map, the particle tunes of the second interval

are plotted and a color code is assigned to the logarithm of the tune variations in the horizontal and vertical plane.

Figures 28 illustrate the frequency maps for the four studies in the LHC (Fig. 28a-28d) and the HL-LHC lattice (Fig. 28e-28h), respectively. The gray lines denote the nominal resonances, i.e., the resonances that intrinsically arise from the non-linear fields such as non-linear magnets and beam-beam effects. In particular, in the absence of noise (Fig. 28a), an important impact is observed due to the third order resonance ($3Q_y = 1$), which is in the vicinity of tune footprint and it affects particles at large amplitudes (red). The second panel of each figure indicates the initial distribution in the horizontal and vertical $x - y$ plane, which is color-coded with the tune diffusion.

From the FMAs, it is observed that the dipolar noise results in an increase of the particles' diffusion, first, by enhancing the strength of some of the nominal resonances and second, through the excitation of additional resonances. In contrast to quadrupolar modulations [44], which lead to the excitation of sideband resonances, the location of the resonances in the presence of a modulated dipolar field error is equal to the frequency of the excitation. As the noise is injected in the horizontal plane, they appear as vertical lines in fixed positions for the low (black) and high (blue) frequency cluster. In particular, the excitations of the high-frequency cluster appear as aliases and, for instance, the excitation at 7.8 kHz in Fig. 28c is located at $f_{\mathrm{rev}} - 7.8$ kHz. For the 50 Hz harmonics in the vicinity of the betatron tune and its alias these additional resonances are located inside the beam's footprint. As shown in the $x - y$ plane, the existence of such resonances impacts both the core and the tails of the distribution. These simulations indicate that the main contributor to the increase of tune diffusion are the spectral components in the high-frequency cluster. The FMAs are an early indicator of the particle's stability and the increase of the tune diffusion due to noise suggests that a decrease of the beam's intensity may be observed (see Section IV C). Due to the coupling of the transverse planes, the strongest dipolar excitations are also visible in the vertical plane, appearing as horizontal lines in the frequency maps. In addition, the modulated dipolar excitations introduce, in the presence of non-linear magnets, also a quadrupolar modulation through feed-down, which explains the sideband resonances that are clearly visible in Fig. 28b and 28f.

Given that these frequency maps are performed in 5D, the modulation induced from the synchrotron motion to the off-momentum particles through chromaticity is not illustrated [44]. This effect leads to the excitation of synchrotron sideband resonances, which overlap with the nominal and the dipolar resonances, further increasing the tune diffusion of the particles in the distribution. The combined effect of dipolar noise and synchro-betatron coupling is included in the DA studies presented in this paper. Furthermore, it must be noted that although the simulations include important non-linearities such as beam-beam, they do not include effects such as electron-cloud, which have been experimentally observed in the LHC [60]. These non-linear fields lead to the excitation of additional resonances, as well, and the interplay between the two effects can lead to a further degradation of the beam performance than the one predicted in these simulations.

C. Simulations of the beam losses

Quantifying the impact of the noise and the non-linearities on the beam intensity evolution requires the tracking of a 6D matched Gaussian distribution. In particular, if impacted by resonances as demonstrated in the previous section, particles at the tails of the distribution close to the limit of DA diffuse and will eventually be lost. Therefore, for these studies, a detailed representation of the tails of the distribution is needed.

To achieve this goal, weighted distributions are employed. The considered initial conditions of the tracked particles form a 4D round and randomly sampled distribution extending up to 6 σ both in the $x - y$ and the $xx'(yy')$-plane. In the longitudinal plane, the momentum deviation of the particles is a uniform distribution that extends up to the limit of the bucket height. To reduce the statistical variations, $9 \cdot 10^4$ particles are tracked in the LHC and HL-LHC lattice in 6D at collision energy for 10^6 turns. In the post-processing, a weight is assigned to each particle according to its initial conditions as computed from the probability density function (PDF) of a Gaussian distribution. In this way, significant statistics is achieved both for the core and the tails of the distribution. However, particles placed at the core of the distribution are assigned a larger weight than the ones at the tails and therefore, their contribution to the computations for losses is more important. Furthermore, a mechanical aperture is defined in the post-processing at 5 σ and particles beyond this threshold are considered lost.

Figure 29 presents the intensity evolution for the LHC (Fig. 29a) and HL-LHC (Fig. 29b) without noise (black), including the 50 Hz harmonics either of the low (blue) or high (orange) frequency cluster and considering both regimes (red). The results shows that, for the time span under consideration, the high-frequency cluster is the main contributor in the increase of losses. These simulations indicate that, based on a lumped transfer function of the noise, the 50 Hz harmonics lead to a reduction of the beam lifetime, which is already visible with a tracking equivalent to 90 seconds of operation. Considering the same noise spectrum for the HL-LHC case shows that a decrease in intensity is also observed. In both cases, the main contributor of proton losses is the high-frequency cluster.

Figure 30 illustrates the intensity evolution in the absence of noise (black), including the noise spectrum of Beam 1 (blue) and 2 (red). The fact that the noise spec-

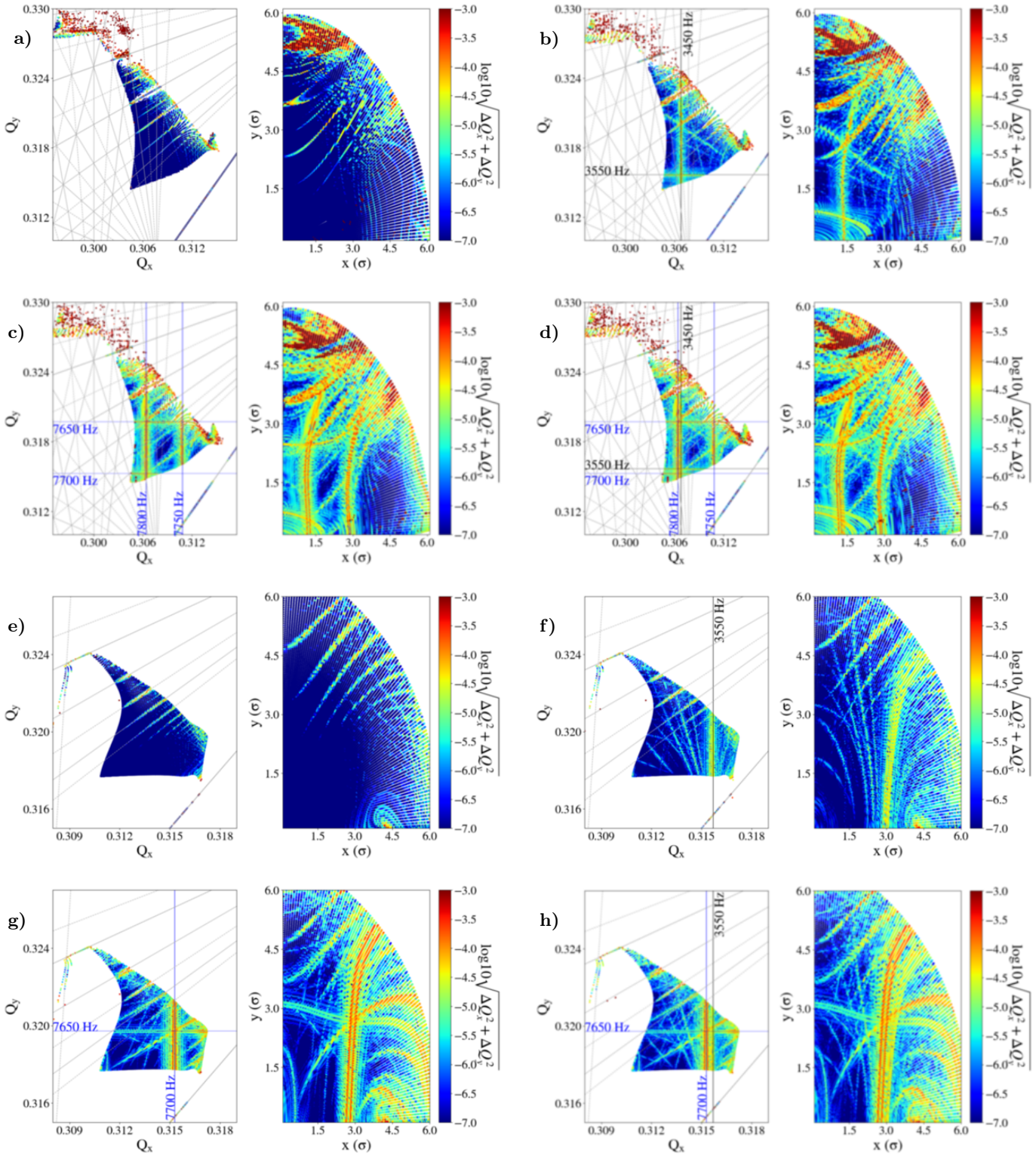

FIG. 28. The frequency maps (left) and the initial configuration space (right) color-coded with the tune diffusion for the LHC (a) in the absence of noise , (b) with noise in the low and (c) high-frequency cluster and (d) combining both regimes. Similar studies are performed for HL-LHC ((e), (f), (g), (h)).

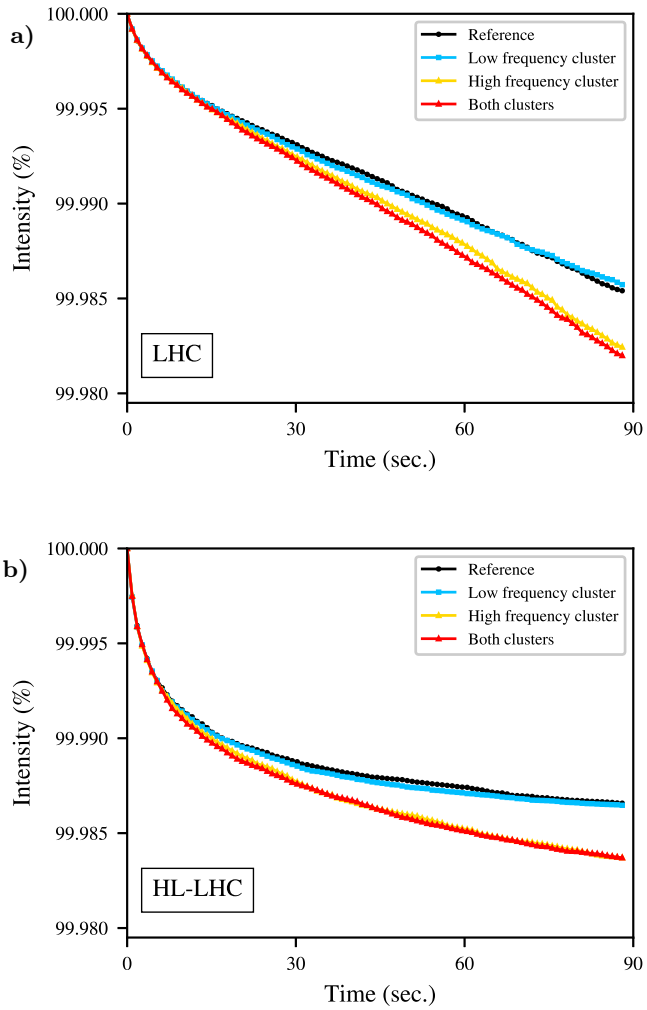

FIG. 29. Intensity evolution for (a) the LHC and (b) the HL-LHC without noise (black), considering only the low (blue) or high (orange) frequency cluster and including the noise in both regimes (red).

trum of Beam 2 is lower by approximately a factor of two compared to Beam 1 results in an asymmetry of the intensity evolution between the two beams. In particular, by fitting the exponential decay of the intensity, a reduction of 23.2% and 6.6% in the lifetime of Beam 1 and 2, respectively, is observed compared to the reference conditions. As a reference, the simulated lifetimes with noise are 158 h and 194 h for Beam 1 and 2, respectively. This observation indicates that, amongst other effects, the noise contributes to the lifetime discrepancy between the two beams that has been observed experimentally.

V. CONCLUSIONS AND DISCUSSION

The purpose of the current study was to investigate the origin of the 50 Hz harmonics, a noise effect that has

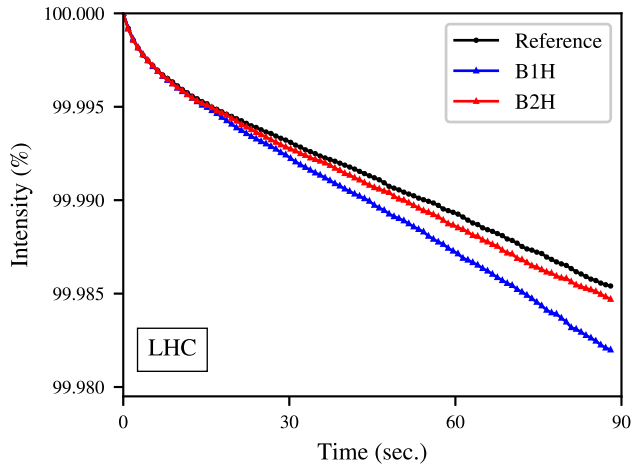

FIG. 30. Intensity evolution for the LHC without noise (black), including the noise spectrum of Beam 1 (blue) and 2 (red).

been observed in the beam signal since the start of the LHC operation. For this reason, a detailed review of the beam spectrum during several beam and machine configurations has been performed that revealed the existence of harmonics in two regimes in the frequency domain: the low-frequency cluster that extends up to 3.6 kHz and the high-frequency cluster at the location $f_{\mathrm{rev}} - f_x$. The methodology presented in this paper allowed us to identify, for the first time in the LHC operation, the existence of the high-frequency cluster on the beam signal.

Based on several observations it is concluded that the two regimes are the result of a real beam excitation. Both clusters consist of 50 Hz harmonics and in both cases, the observed effect exhibits a dipolar nature with a similar signature in frequency domain. In terms of amplitude, an asymmetry between the two clusters has been identified. In particular, more significant excitation amplitudes are reported for the high-frequency cluster, an effect that contradicts the expected attenuation of the power converter noise with increasing frequency. It must also be mentioned that, during the proton run of 2018, the measured effect of the noise in the horizontal plane of Beam 1 was a factor two larger than the one of Beam 2.

As far as the low-frequency cluster is concerned, a correlation with the eight thyristor, line-commutated power converters of the Main Bends is established, through experiments with the active filters. It is concluded that the power converters of the main dipoles are the major contributor to the appearance of the low-frequency cluster in the transverse beam spectrum and therefore, the noise is distributed in all the LHC dipoles. It is the first time that such a correlation has been demonstrated in the LHC operation.

The low and high-frequency clusters exhibit a similar signature in frequency domain: first, they consist of multiple 50 Hz harmonics and second, a common phase mod-

ulation is observed for all the harmonics, which originates from the stability of the electrical network mains. These findings indicate that the low and high-frequency clusters emerge from a common source. However, various observations, such as the amplitude asymmetry between the low and high-frequency cluster, suggest that the latter results from the interplay between noise from the dipoles and a mechanism originating from the beam rather than a direct excitation. Therefore, future studies will focus on identifying the mechanism that increases the sensitivity of the beam to noise in the regime $f_{\mathrm{rev}} - f_x$ compared to f_x.

Single-particle tracking simulations, based on a realistic noise spectrum and a simplified lumped transfer function of the noise, indicate that these excitations increase the diffusion of the particles. From a tracking that corresponds to 90 seconds in operation, the excitation of additional resonances eventually led to proton losses, especially due to the high-frequency cluster. Based on these results, it is concluded that the 50 Hz harmonics had an impact on the beam performance during the LHC operation.

In addition, due to the discrepancy of the noise spectrum in Beam 1 and 2, the aforementioned simulations illustrated a clear discrepancy in the intensity evolution of the two beams. An important lifetime asymmetry between the two beams has been observed since the beginning of run 2 and it is the first time that tracking simulations show that noise can contribute to this effect.

In the context of this study, a general analysis framework of the experimental and simulation data has been developed. In particular, this paper presented a method to compute high-bandwidth spectra from bunch-by-bunch acquisitions, while preserving the metric and reducing the noise floor with signal averaging. Moreover, we introduced several methods to determine whether a perturbation in the beam spectrum is a real beam excitation or a spurious signal entering its path. In terms of simulations, this paper illustrated potential ways to define an acceptable noise threshold for operation through DA scans. These scans were used to verify the validity of our simulation tools including noise against experimental observations with controlled excitations. Finally, a method to determine the intensity evolution of a distribution with a detailed representation of its tails using weights has been demonstrated. The methods of analysis presented in this paper can be applied to studies of other types of noise effects, both from the experimental and simulation point of view.

In conclusion, this study improves our understanding of the noise effects that were present during the LHC operation. Due to the origin of the noise effect under investigation, the 50 Hz harmonics will be an issue for the future operation of the LHC. Therefore, the studies will focus on identifying the mechanism that not only enables this high-frequency perturbation to affect the beam motion but that also leads to such a significant impact compared to the direct excitations of the low-frequency cluster. More importantly, regardless of the source, mitigation measures should be considered in future operation to further suppress the 50 Hz harmonics from the beam motion.

ACKNOWLEDGMENTS

The authors gratefully acknowledge H. Bartosik, X. Buffat, J.-P. Burnet, L. R. Carver, R. De Maria, D. Gamba, M. Martino, V. Montabonnet, N. Mounet, D. Nisbet, H. Thiesen, Y. Thurel and J. Wenninger for valuable suggestions and discussions on this work. We would like to thank D. Valuch and M. Soderen for all ADT related measurements and experiments, T. Levens for the MIM measurements and discussions, M. C. Bastos and C. Baccigalupi for the power converter acquisitions and discussions, J. Olexa for the DOROS measurements and S. Uznanski for the DCCTs acquisitions.

Appendix A: Beam spectrum from bunch-by-bunch acquisitions

In the presence of a regular filling scheme, the bunch-by-bunch and turn-by-turn ADTObsBox data can be combined to increase the effective bandwidth of the instrument. Signal averaging is not only needed to access the high-frequency components of the signal without aliasing, but also to reduce the noise floor of the spectrum compared to the single bunch case. In particular, averaging the signals of N_b bunches yields a $\sqrt{N_b}$ increase in the signal to noise ratio, in the presence of random noise with zero mean that is uncorrelated with the signal [61].

The spectrum of individual bunches and after averaging over all the bunches in the machine is shown in Fig. 31 for the horizontal plane of Beam 1, for a physics fill and a window length of $4 \cdot 10^4$ turns. The colored lines show the envelope of the spectra of several individual bunches, which is computed by setting a parametric peak threshold of $2 \cdot 10^{-3}$ σ. The single bunch noise floor is several orders of magnitude higher than the 50 Hz harmonics and thus, signal averaging is necessary.

The time delay Δt_i of a trailing bunch i with respect to the first bunch in the machine, considered as the reference, results in a phase angle $\Delta\phi_i = 2\pi f \Delta t_i$, where f is the frequency under consideration. Consequently, the dephasing of the signals across the ring is proportional to the frequency and the longitudinal spacing of the bunches in the machine. To illustrate this effect, three trains of 48 bunches are considered in simulations with a dipolar excitation at 3 kHz. The bunch spacing is 25 ns and the trains are equally spaced in the LHC ring. The complex spectrum is computed for each bunch and the phase evolution of the 3 kHz line is extracted. Figure 32 depicts the phase evolution of the excitation for the three trains as a function of the bunch position in the ring. The color code represents the bunch number and the gray line is

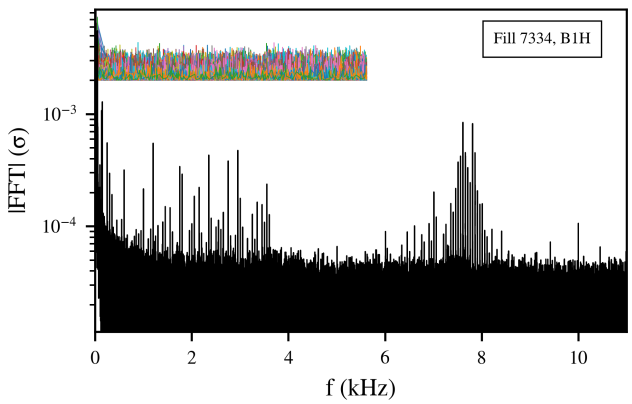

FIG. 31. The spectral envelope of several individual bunches (colored lines) and the spectrum after averaging over all the bunches in the machine (black).

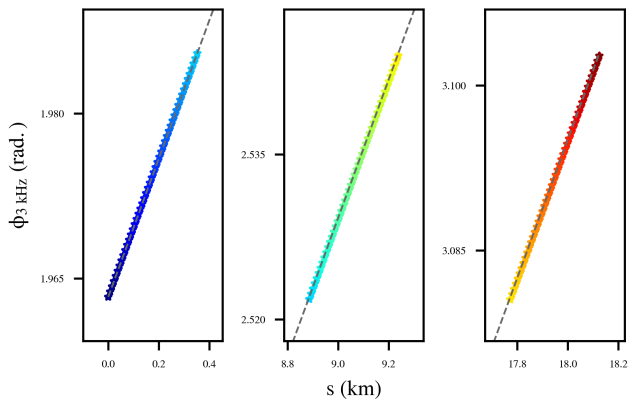

FIG. 32. Phase evolution of the excitation at 3 kHz as a function of the bunch position for three trains of 48 bunches in the LHC ring. The dashed gray line represents the expected dephasing.

the expected phase evolution. The linear phase evolution of an excitation across the trains in the machine has been experimentally verified by injecting noise with the transverse damper kicker (see Appendix D 1).

For frequencies much lower than the sampling frequency ($f \ll f_{\mathrm{rev}}$), the dephasing is negligible and the bunch-by-bunch data can be directly averaged in time domain. For frequencies comparable to the revolution frequency, such as the high-frequency cluster, the dephasing between the bunches cannot be neglected. In this case, simply averaging the bunch-by-bunch information will lead to an error in the resulting metric. To illustrate this effect, the first bunches of the three trains are selected. Figure 33 illustrates the spectra for the first bunches (Fig. 33a) of the first (black), second (blue) and third (green) train, respectively, in the presence of a dipolar excitation at 3 kHz. The excitation results in an offset of 13.9 μm (red dashed line), while the second peak corresponds to the betatron tune. Then, the complex Fourier

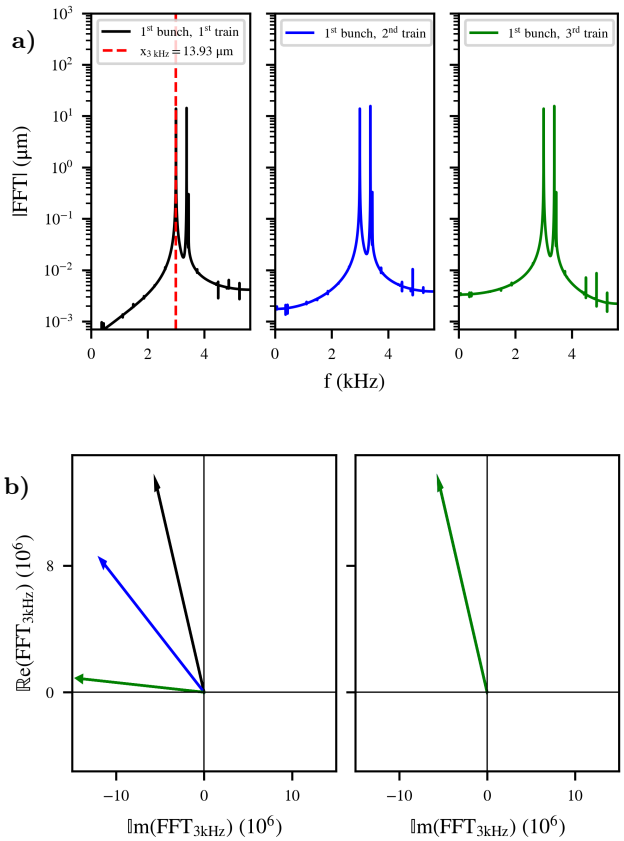

FIG. 33. (a) Spectrum of the first bunches of the first (black), second (blue) and third (green) train in the presence of a dipolar excitation at 3 kHz (red dashed line). (b) Phase of the excitation for the three bunches before (left) and after (right) the correction.

coefficients at 3 kHz are computed. Figure 33b presents the vector of the excitation in the spectrum, whose angle corresponds to the phase, for each bunch (left). For a filling scheme consisting of three trains located in azimuthally symmetric locations in the ring, the dephasing at 3 kHz is important. Averaging over the three vectors without correcting for the dephasing will lead to an error in the offset of the final spectrum. To this end, an algorithm that applies a phase correction has been implemented. The steps of the method are the following: first, the complex spectra $F_i(\omega)$ are computed for each bunch, where $\omega = 2\pi f$. Then, a rotation is applied which is proportional to the time delay Δt_i and the frequencies f of the spectrum. The impact of the rotation is depicted in the second plot of Fig. 33b. Finally, the average over all bunches is computed. The procedure is described by the following expression:

$$F(\omega) = \frac{1}{N_b} \sum_{i=1}^{N_b} F_i(\omega) \mathrm{e}^{-j\omega\Delta t_i}. \tag{A1}$$

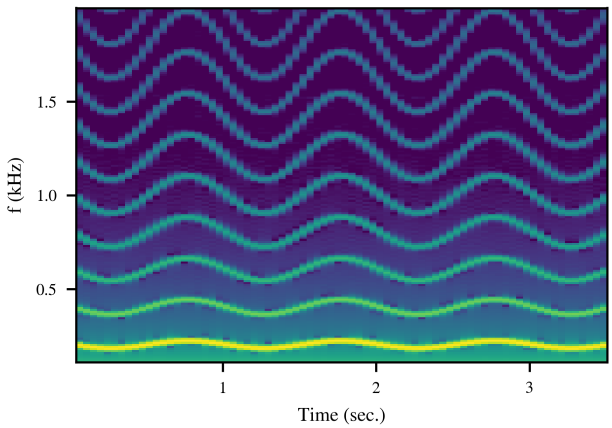

FIG. 34. The impact of a frequency modulation on a harmonic dipolar excitation.

Appendix B: Impact of a frequency modulation of the fundamental frequency on its harmonics

This section presents the impact of a frequency modulation on a harmonic dipolar excitation, similar to the one observed in the 50 Hz harmonics. To simulate this effect, a single particle is tracked in the LHC lattice in the presence of a dipole field error. The dipole strength is modulated with the absolute value of a sinusoidal function at a frequency of 100 Hz. This perturbation mimics a non-linear transfer function exciting all the even harmonics of the fundamental frequency (100 Hz). Furthermore, an arbitrary low-frequency modulation is injected in the fundamental frequency. Figure 34 illustrates the spectrogram for a frequency range up to 1.8 kHz, color-coded with the PSD. All harmonics experience a similar frequency modulation with a peak-to-peak variation proportional to the order of the harmonic.

Appendix C: Analytical formalism for a modulated dipolar field error

In a circular accelerator, the kick related to a modulated dipolar field error Θ_p with a deflection θ_p and a frequency of Q_p oscillations per turn can be represented as:

$$\bar{P}_n = \begin{pmatrix} 0 \\ \Theta_p(n) \end{pmatrix} = \begin{pmatrix} 0 \\ \theta_p \cos\left(2\pi Q_p n\right) \end{pmatrix}, \tag{C1}$$

where n is the turn considered. In the linear approximation, i.e., for a deflection much smaller than the beam size, considering only the horizontal motion in the normalized phase space and assuming that the noise source and the observation point are situated in the same location, the position of a given particle can be expressed as:

$$\bar{X}_N = \begin{pmatrix} \bar{x}_N \\ \bar{x}'_N \end{pmatrix} = \sum_{n=-\infty}^{N} M^{N-n} \bar{P}_n, \tag{C2}$$

where $\bar{X}_N$ is the vector representation of the position and momentum at turn N and M is the linear rotation with:

$$M^N = \begin{pmatrix} \cos(2\pi QN) & \sin(2\pi QN) \\ -\sin(2\pi QN) & \cos(2\pi QN) \end{pmatrix}, \tag{C3}$$

where Q is the machine betatron tune. Combining Eq. (C1), (C2) and (C3) and assuming that the perturbation is present from $n \to -\infty$, it yields:

$$\begin{cases} \bar{x}_N = \sum_{n=-\infty}^{N} \Theta_p(n) \sin\left(2(N-n)\pi Q\right) \\ \bar{x}'_N = \sum_{n=-\infty}^{N} \Theta_p(n) \cos\left(2(N-n)\pi Q\right). \end{cases} \tag{C4}$$

Combining Eq. (C1) and (C4) and computing the convergence of the series, the closed form expression of the offset induced by the modulated dipolar kick is:

$$\bar{x}_N = \frac{\theta_p \cos\left(2\pi N Q_p\right) \sin\left(2\pi Q\right)}{2\left(\cos\left(2\pi Q_p\right) - \cos(2\pi Q)\right)}. \tag{C5}$$

In physical coordinates, the maximum offset observed at the position s is equal to:

$$|x_{\max,N}(s)| = \left| \frac{\sqrt{\beta(s)\beta_p}\ \theta_p \sin\left(2\pi Q\right)}{2\left(\cos\left(2\pi Q_p\right) - \cos(2\pi Q)\right)} \right|, \tag{C6}$$

where β_p is the β-function at the position of the perturbation. A comparison between the results of simulations and Eq. (C6) is performed as a sanity check. A single particle is tracked in the LHC lattice, in the presence of a dipolar modulation. The amplitude of the kick is 1 nrad and the frequency varies across the studies. The offset is computed from the particle's spectrum for each study and is then compared to the analytical formula. Figure 35 illustrates the offset as a function of the frequency computed analytically (black) and from simulations (blue) and a very good agreement is found between the two. For a constant excitation amplitude, a resonant behavior is expected as the frequency approaches to $k \cdot f_{\text{rev}} \pm f_x$, where k is an integer.

As a reference, the maximum offset observed in the beam spectrum is equal to $0.84 \cdot 10^{-3}\sigma$ for a normalized emittance of $\epsilon_n = 2$ μm rad, a beam energy of 6.5 TeV and a $\beta-$function equal to 105 m. Considering a single dipolar excitation at the location of the observation point, Fig. 36 shows that the equivalent kick, as computed from Eq. (C6), is $\theta_p = 0.09$ nrad for $Q = 0.31$ and $|Q - Q_p| = 5 \cdot 10^{-3}$.

The β-functions at the location of the ADTObsBox Q7 pickup for both beams and planes, at injection and Stable Beams can be found in Table V.

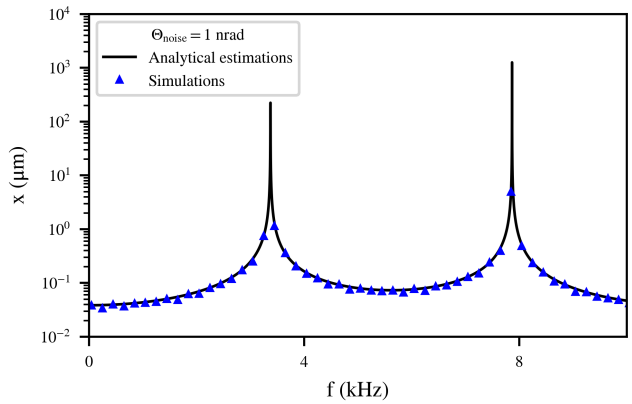

FIG. 35. The offset as a function of the dipolar excitation frequency with $\theta = 1$ nrad as computed from the closed form (black) and from simulations (blue).

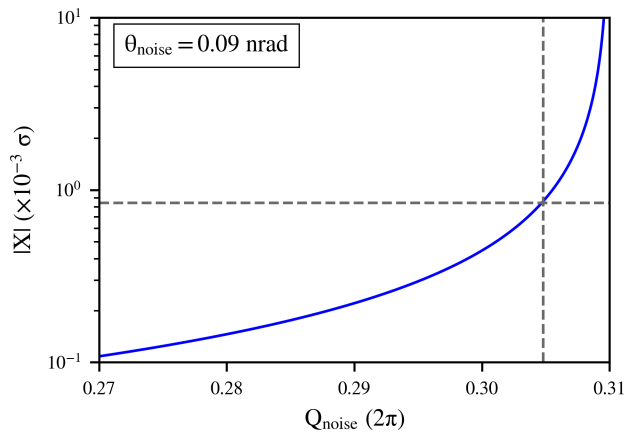

FIG. 36. The horizontal offset as a function of the noise tune for a betatron tune and a deflection equal to 0.31 and 0.09 nrad, respectively. The gray lines illustrate the maximum offset that has been observed experimentally.

TABLE V. The β-functions at the position of the Q7 pickup per beam and plane with injection and collision optics ($\beta^* = 30\ cm$).

	Plane	β at injection (m)	β at collision (m)
Beam 1	Horizontal	130.9	100.7
Beam 1	Vertical	173.6	99.6
Beam 2	Horizontal	151.1	109.6
Beam 2	Vertical	166.3	166.3

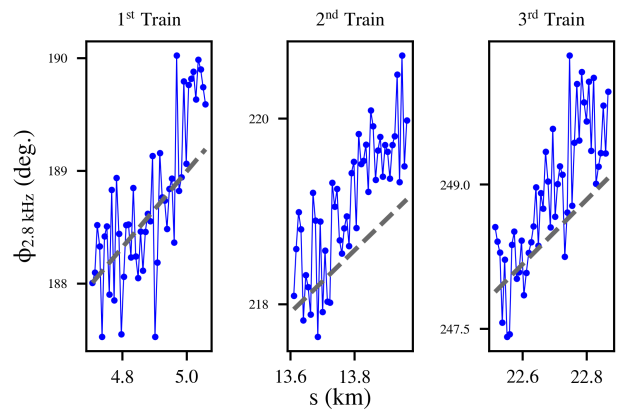

FIG. 37. The bunch-by-bunch phase evolution of an excitation at 2.8 kHz, which led to an offset of 7.9 μm, as a function of the position of the three trains in the ring. The expected dephasing is illustrated with the gray dashed line.

Appendix D: Observations during controlled excitations

1. Phase evolution of the noise in the ring

The method to average over multiple bunches presented in Appendix A is based on the assumption that the dephasing of the bunch-by-bunch spectra is linearly proportional to the frequencies and the time delay of the trailing bunches compared to the reference, i.e., the first bunch in the machine. Although this hypothesis has been validated with simulations, experimentally, with the present ADTObsBox noise baseline, the bunch-by-bunch phase evolution of the harmonics cannot be directly computed. On the contrary, in the presence of a strong excitation, the determination of the bunch-by-bunch phase evolution is feasible as the amplitude of the noise line exceeds the noise floor of the single bunch spectrum. To this end, the bunch-by-bunch Fourier spectrum is computed during an excitation at 2.8 kHz in the horizontal plane of Beam 1, which resulted in an offset of 7.9 μm. Figure 37 demonstrates the phase evolution of the excitation (blue) across the three trains. A comparison with the expected phase evolution (gray dashed line) yields that a good agreement is found between experimental observations and predictions.

2. Coupling of the noise

The controlled excitations can improve the understanding on the role of the coupling in the presence of noise. Figure 38 illustrates the spectrum of the horizontal (magenta) and the vertical (cyan) plane of Beam 1 during an excitation at 600 Hz in the single-bunch fill. During this time interval, despite the fact that only the horizontal plane was excited, the excitation is also visi-

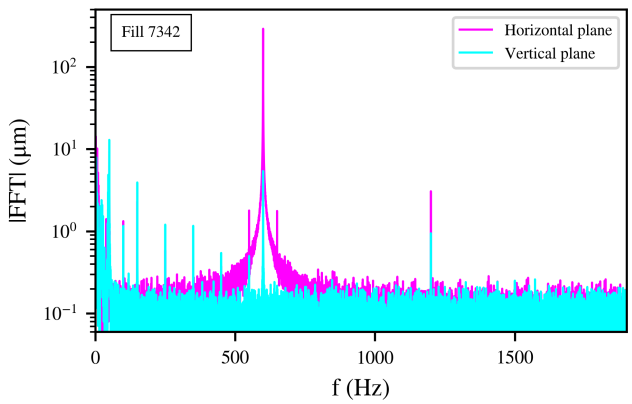

FIG. 38. The impact of a horizontal controlled excitation at 600 Hz for the horizontal (magenta) and vertical (cyan) plane of Beam 1.

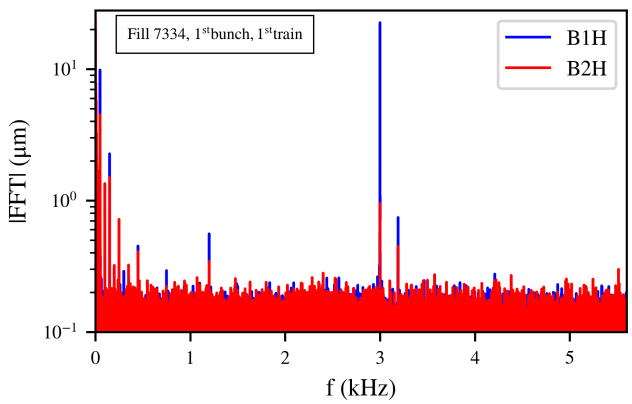

FIG. 39. The horizontal spectrum of Beam 1 (blue) and 2 (red) during an excitation at 3 kHz, applied only in Beam 1, with a filling scheme consisting of multiple trains.

ble in the vertical plane. In particular, after normalizing the observed offsets with the corresponding β-functions, the comparison between the two planes yields that the vertical offset is 1.6% of the horizontal one.

An similar excitation at 600 Hz was applied only in Beam 1 with multiple trains injected in the ring. It must be noted that, based on the selected filling scheme, the two beams encounter at IP1 and 5. Figure 39 depicts the spectrum of Beam 1 (blue) and 2 (red) for the first bunch of the first train. Although the excitation was applied only in Beam 1, it was also visible in Beam 2, an effect that was not observed during the single-bunch fill.

As the amplitude of the excitation exceeds the single-bunch noise baseline, the bunch-by-bunch variations of the injected noise can be computed. Figure 40 presents the amplitude evolution of the excitation as a function of the bunch position in the ring for Beam 1 (Fig. 40a) and 2 (Fig. 40b). The excitation is visible in Beam 2, although only Beam 1 was excited. In fact, the bunch-by-bunch variations observed in Beam 2 indicate that a maximum

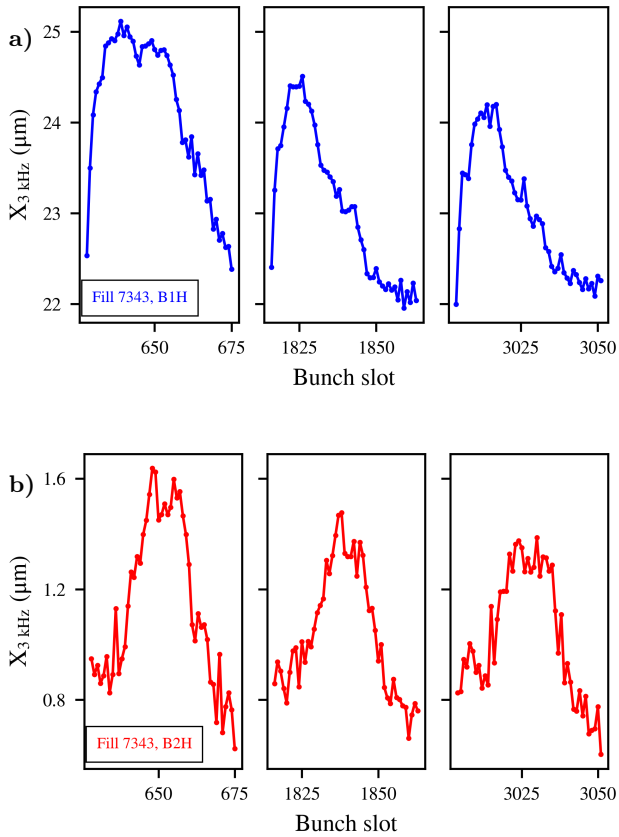

FIG. 40. The bunch-by-bunch variations of the excitation at 3 kHz for (a) Beam 1 and (b) Beam 2.

impact is observed at the center of the train. This effect is consistent with coupling through beam-beam effects as the number of long-range encounters in IP1 and 5 is maximum at the center of the trains.

[1] T. J. Satogata, *Nonlinear resonance islands and modulational effects in a proton synchrotron*, Ph.D. thesis, Northwestern U. (1993).

[2] F. Zimmermann, *Emittance growth and proton beam lifetime in HERA*, Ph.D. thesis, Hamburg U. (1993).

[3] O. S. Brüning and F. Willeke, Diffusion-like processes in proton storage rings due to the combined effect of nonlinear fields and modulational effects with more than one frequency, in *European Particle Accelerator Conference (EPAC 1994)* (1994).

[4] O. S. Brüning, M. Seidel, K. Mess, and F. Willeke, *Measuring the effect of an external tune modulation on the particle diffusion in the proton storage ring of HERA*, Tech. Rep. (P00021147, 1994).

[5] O. S. Brüning, P. Collier, P. Lebrun, S. Myers, R. Ostojic, J. Poole, and P. Proudlock, *LHC Design Report*, CERN Yellow Reports: Monographs (CERN, Geneva, 2004).

[6] M. Kuhn, G. Arduini, J. Emery, A. Guerrero, W. Hofle, V. Kain, F. Roncarolo, M. Sapinski, M. Schaumann, and R. Steinhagen, LHC Emittance preservation during the 2012 run., in *Proceedings, 4th Evian Workshop on LHC beam operation: Evian Les Bains, France, December 17-20, 2012* (2012) pp. 161–170. 10 p.

[7] S. Cettour Cave, R. De Maria, M. Giovannozzi, M. Ludwig, A. MacPherson, S. Redaelli, F. Roncarolo, M. Solfaroli Camillocci, and W. Venturini Delsolaro, Non-linear beam dynamics tests in the LHC: Measurement of intensity decay for probing dynamic aperture at injection (2013).

[8] G. Arduini, 50 Hz lines studies: First observations, `https://indico.cern.ch/event/436679/contributions/1085928` (2015), accessed: 2019-12-13.

[9] R. De Maria, Observation of 50 Hz lines in the LHC BBQ system, `https://lhc-beam-operation-committee.web.cern.ch/lhc-beam-operation-committee` (2012), accessed: 2019-12-14.

[10] T. Linnecar and W. Scandale, *Phenomenology and causes of the 50 Hz spaced lines contaminating the Schottky signal*, Tech. Rep. CERN-SPS-DI-MST-TL-WS-EEK. CERN-SPS-Improvement-Report-203 (CERN, Geneva, 1986).

[11] X. Altuna, C. Arimatea, R. Bailey, T. Bohl, D. Brandt, K. Cornelis, C. Depas, F. Galluccio, J. Gareyte, R. Giachino, M. Giovannozzi, Z. Guo, W. Herr, A. Hilaire, T. Lundberg, J. Miles, L. Normann, T. Risselada, W. Scandale, F. Schmidt, A. Spinks, M. Venturini, M. Giovannozzi, and F. Schmidt, The 1991 dynamic aperture experiment at the CERN SPS, AIP Conference Proceedings **255**, 355 (1992), https://aip.scitation.org/doi/pdf/10.1063/1.42289.

[12] O. S. Brüning, Diffusion in a FODO cell due to modulation effects in the presence of nonlinear fields, Part. Accel. **41**, 133 (1992).

[13] W. Fischer and M. Giovannozzi, Dynamic aperture experiment at a synchrotron, Physical Review E **55**, 3507 (1997).

[14] M. Gasior and R. Jones, *The principle and first results of betatron tune measurement by direct diode detection*, Tech. Rep. LHC-Project-Report-853. CERN-LHC-Project-Report-853 (CERN, Geneva, 2005) revised version submitted on 2005-09-16 09:23:15.

[15] O. S. Brüning, M. Seidel, K. Mess, and F. Willeke, *Measuring the effect of an external tune modulation on the particle diffusion in the proton storage ring of HERA*, Tech. Rep. (P00021147, 1994).

[16] O. S. Brüning and F. Willeke, Reduction of particle losses in HERA by generating an additional harmonic tune modulation, in *Proceedings Particle Accelerator Conference*, Vol. 1 (1995) pp. 420–422 vol.1.

[17] P. Cameron, M. Gasior, R. Jones, and C. Tan, *The effects and possible origins of mains ripple in the vicinity of the betatron spectrum.*, Tech. Rep. (Brookhaven National Lab.(BNL), Upton, NY (United States), 2005).

[18] P. Cameron, M. Gasior, R. Jones, and C. Tang, *Observations of direct excitation of the betatron spectrum by mains harmonics in RHIC*, Tech. Rep. (Brookhaven National Laboratory (BNL) Relativistic Heavy Ion Collider, 2006).

[19] C.-Y. Tan, Novel tune diagnostics for the Tevatron, in *Proceedings of the 2005 Particle Accelerator Conference* (IEEE, 2005) pp. 140–144.

[20] V. Shiltsev, G. Stancari, and A. Valishev, Ambient betatron motion and its excitation by "ghost lines" in Tevatron, Journal of Instrumentation **6** (08), P08002.

[21] G. Apollinari, I. Béjar Alonso, O. Brüning, P. Fessia, M. Lamont, L. Rossi, and L. Tavian, High-Luminosity Large Hadron Collider (HL-LHC), CERN Yellow Rep. Monogr. **4**, 1 (2017).

[22] M. Solfaroli Camillocci, S. Redaelli, R. Tomás, and J. Wenninger, Combined Ramp and Squeeze to 6.5 TeV in the LHC, in *Proceedings, 7th International Particle Accelerator Conference (IPAC 2016): Busan, Korea, May 8-13, 2016* (2016) p. TUPMW031.

[23] S. Fartoukh, Achromatic telescopic squeezing scheme and application to the LHC and its luminosity upgrade, Phys. Rev. ST Accel. Beams **16**, 111002 (2013).

[24] B. Muratori and T. Pieloni, Luminosity levelling techniques for the LHC (2014) pp. 177–181. 5 p, comments: 5 pages, contribution to the ICFA Mini-Workshop on Beam-Beam Effects in Hadron Colliders, CERN, Geneva, Switzerland, 18-22 Mar 2013.

[25] N. Karastathis, K. Fuchsberger, M. Hostettler, Y. Papaphilippou, and D. Pellegrini, Crossing angle anti-leveling at the LHC in 2017, in *Journal of Physics: Conference Series*, Vol. 1067 (IOP Publishing, 2018) p. 022004.

[26] M. Gasior, Faraday cup award: High sensitivity tune measurement using direct diode detection, Conf. Proc. **C1204151**, MOAP02. 7 p (2012).

[27] O. Jones, LHC beam instrumentation, in *2007 IEEE Particle Accelerator Conference (PAC)* (IEEE, 2007) pp. 2630–2634.

[28] L. Carver, X. Buffat, A. Butterworth, W. Höfle, G. Iadarola, G. Kotzian, K. Li, E. Métral, M. Ojeda Sandonís, M. Söderén, and D. Valuch, Usage of the transverse damper observation box for high sampling rate transverse position data in the LHC, in *8th Int. Particle Accelerator Conf. (IPAC'17), Copenhagen, Denmark, May 2017*, CERN-ACC-2017-117 (2017) pp. 389–392.

[29] M. Ojeda Sandonís, P. Baudrenghien, A. Butterworth, J. Galindo, W. Höfle, T. Levens, J. Molendijk, F. Vaga, and D. Valuch, Processing high-bandwidth bunch-by-bunch observation data from the RF and transverse damper systems of the LHC, in *Proceedings, 15th International Conference on Accelerator and Large Experimental Physics Control Systems (ICALEPCS 2015): Melbourne, Australia, October 17-23, 2015* (2015) p. WEPGF062.

[30] M. Söderén, G. Kotzian, M. Ojeda Sandonís, and D. Valuch, Online bunch by bunch transverse instability detection in LHC, in *Proceedings, 8th International Particle Accelerator Conference (IPAC 2017): Copenhagen, Denmark, May 14-19, 2017* (2017) p. MOPAB117.

[31] T. Persson, J. M. Coello de Portugal, A. Garcia-Tabares, M. Gąsior, A. Langner, T. Lefèvre, E. Maclean, L. Malina, J. Olexa, P. Skowroński, and R. Tomás, Experience with DOROS BPMs for coupling measurement and correction, in *7th Int. Particle Accelerator Conf.(IPAC'16), Busan, Korea, May 8-13, 2016* (JACOW, Geneva, Switzerland, 2016) pp. 303–305.

[32] J. Olexa, O. Ondracek, Z. Brezovic, and M. Gasior, *Prototype system for phase advance measurements of LHC small beam oscillations*, Tech. Rep. CERN-ATS-2013-038

(CERN, Geneva, 2013).

[33] R. Steinhagen, T. Lucas, and M. Boland, A Multiband-Instability-Monitor for high-frequency intra-bunch beam diagnostics (2013).

[34] T. Levens, T. Lefèvre, and D. Valuch, Initial results from the LHC Multi-Band Instability Monitor, in *Int. Beam Instrumentation Conf.(IBIC'18), Shanghai, China, 09-13 September 2018* (JACOW Publishing, Geneva, Switzerland, 2019) pp. 314–318.

[35] H. Nyquist, Certain topics in telegraph transmission theory, Transactions of the American Institute of Electrical Engineers **47**, 617 (1928).

[36] O. S. Brüning, P. Collier, P. Lebrun, S. Myers, R. Ostojic, J. Poole, and P. Proudlock, *LHC Design Report*, CERN Yellow Reports: Monographs (CERN, Geneva, 2004) Chap. Power converter system.

[37] H. Thiesen, G. Hudson, D. Nisbet, V. Montabonnet, M. Bastos, S. Page, and Q. King, High precision current control for the LHC main power converters, in *Conf. Proc.*, IPAC-2010-WEPD070 (2010) p. WEPD070.

[38] S. Kostoglou, N. Karastathis, Y. Papaphilippou, D. Pellegrini, and P. Zisopoulos, Development of computational tools for noise studies in the LHC, in *Conf. Proc.*, IPAC-2017-THPAB044 (2017) p. THPAB044.

[39] J. Laskar, C. Froeschlé, and A. Celletti, The measure of chaos by the numerical analysis of the fundamental frequencies. application to the standard mapping, Physica D: Nonlinear Phenomena **56**, 253 (1992).

[40] M. Buzio, P. Galbraith, S. Gilardoni, D. Giloteaux, G. Golluccio, C. Petrone, L. Walckiers, and A. Beaumont, Development of upgraded magnetic instrumentation for CERN's real-time reference field measurement systems, *Proceedings, 1st International Particle Accelerator Conference (IPAC'10): Kyoto, Japan, May 23-28, 2010*, Conf. Proc. **C100523**, MOPEB016 (2010).

[41] T. Bohl, Functional specification for upgrade of SPS B-train, CERN, Geneva, Switzerland, Rep. EDMS **1689759** (2016).

[42] A. Huschauer, A. Blas, J. Borburgh, S. Damjanovic, S. Gilardoni, M. Giovannozzi, M. Hourican, K. Kahle, G. Le Godec, O. Michels, G. Sterbini, and C. Hernalsteens, Transverse beam splitting made operational: Key features of the multiturn extraction at the CERN Proton Synchrotron, Phys. Rev. Accel. Beams **20**, 061001 (2017).

[43] H. Thiesen and D. Nisbet, Review of the initial phases of the LHC power converter commissioning, *Particle accelerator. Proceedings, 11th European Conference, EPAC 2008, Genoa, Italy, June 23-27, 2008*, Conf. Proc. **C0806233**, THPP132 (2008).

[44] S. Kostoglou, H. Bartosik, Y. Papaphilippou, G. Sterbini, and N. Triantafyllou, Tune modulation effects in the high luminosity large hadron collider (2020), arXiv:2003.00960 [physics.acc-ph].

[45] N. Karastathis, S. Fartoukh, S. Kostoglou, Y. Papaphilippou, M. Pojer, A. Poyet, M. Solfaroli Camillocci, and G. Sterbini, *MD 3584: Long-Range Beam-Beam 2018*, Tech. Rep. (CERN, 2020).

[46] A. Verweij, V. Baggiolini, A. Ballarino, B. Bellesia, F. Bordry, A. Cantone, M. Casas Lino, A. Serra, C. Trello, N. Catalan Lasheras, Z. Charifoulline, G. Coelingh, K. Dahlerup-Petersen, G. D'Angelo, R. Denz, S. Feher, R. Flora, M. Gruwé, V. Kain, and M. Zerlauth, Performance of the main dipole magnet circuits of the LHC during commissioning, EPAC 2008 - Contributions to the Proceedings (2008).

[47] O. S. Brüning, P. Collier, P. Lebrun, S. Myers, R. Ostojic, J. Poole, and P. Proudlock, Power converter system, in *LHC Design Report*, CERN Yellow Reports: Monographs (CERN, Geneva, 2004) Chap. 10, pp. 275–307.

[48] J.-P. Burnet, Test results of RPTE LHC thyristor rectifier with active filter (2019), unpublished.

[49] F. Dubouchet, W. Hofle, G. Kotzian, and D. Valuch, "What you get" - Transverse damper, in *Proceedings, 4th Evian Workshop on LHC beam operation: Evian Les Bains, France, December 17-20, 2012*, CERN (CERN, Geneva, 2012) pp. 73–78.

[50] J. P. O. Komppula, G. Kotzian, S. Rains, M. Söderén, and D. Valuch, ADT and ObsBox in LHC Run 2, plans for LS2, in *Proceedings, 9th Evian Workshop on LHC beam operation: Evian Les Bains, France, January, 2019* (2019).

[51] M. Morrone, M. Martino, R. De Maria, M. Fitterer, and C. Garion, Magnetic frequency response of High-Luminosity Large Hadron Collider beam screens, Phys. Rev. Accel. Beams **22**, 013501 (2019).

[52] F. Ruggiero, Single beam collective effects in the LHC, *Collective effects in large hadron colliders. Proceedings, International Workshop, Montreux, Switzerland, October 17-22, 1994*, Part. Accel. **50**, 83 (1995).

[53] SixTrack, `http://sixtrack.web.cern.ch/SixTrack/` (2019), accessed: 2019-11-26.

[54] R. D. Maria, J. Andersson, V. K. B. Olsen, L. Field, M. Giovannozzi, P. D. Hermes, N. Høimyr, S. Kostoglou, G. Iadarola, E. Mcintosh, A. Mereghetti, J. W. Molson, D. Pellegrini, T. Persson, M. Schwinzerl, E. H. Maclean, K. Sjobak, I. Zacharov, and S. Singh, SixTrack project: Status, runtime environment, and new developments, in *Proceedings, 13th International Computational Accelerator Physics Conference, ICAP2018: Key West, FL, USA, 20-24 October 2018* (2019) p. TUPAF02.

[55] P. Burla, D. Cornuet, K. Fischer, P. Leclère, and F. Schmidt, *Power supply ripple study at the SPS*, Tech. Rep. CERN-SL-94-11-AP (CERN, Geneva, 1994).

[56] Y. Papaphilippou, Detecting chaos in particle accelerators through the frequency map analysis method, Chaos: An Interdisciplinary Journal of Nonlinear Science **24**, 024412 (2014).

[57] J. Laskar, Introduction to frequency map analysis, in *Hamiltonian systems with three or more degrees of freedom* (Springer, 1999) pp. 134–150.

[58] J. Laskar, Frequency map analysis and particle accelerators, in *Proceedings of the 2003 Particle Accelerator Conference*, Vol. 1 (IEEE, 2003) pp. 378–382.

[59] J. Laskar, Application of frequency map analysis, in *The Chaotic Universe: Proceedings of the Second ICRA Network Workshop, Rome, Pescara, Italy, 1-5 February 1999*, Vol. 10 (World Scientific, 2000) p. 115.

[60] A. Romano, O. Boine-Frankenheim, X. Buffat, G. Iadarola, and G. Rumolo, Electron cloud buildup driving spontaneous vertical instabilities of stored beams in the Large Hadron Collider, Phys. Rev. Accel. Beams **21**, 061002 (2018).

[61] U. Hassan and S. Anwar, Reducing noise by repetition: Introduction to signal averaging, European Journal of Physics **31**, 453 (2010).